







# Influence of orographic precipitation on coevolving landforms and vegetation in semi-arid ecosystems

Ankur Srivastava<sup>1,2</sup>  | Omer Yetemen<sup>1,3</sup>  | Patricia M. Saco<sup>1</sup>  |  
Jose F. Rodriguez<sup>1</sup>  | Nikul Kumari<sup>1,2</sup>  | Kwok P. Chun<sup>4</sup> 

<sup>1</sup>Centre for Water Security and Environmental Sustainability and School of Engineering, The University of Newcastle, Callaghan, Australia

<sup>2</sup>Faculty of Science, University of Technology Sydney, Sydney, Australia

<sup>3</sup>Eurasia Institute of Earth Sciences, Istanbul Technical University, Istanbul, Turkey

<sup>4</sup>Department of Geography, Hong Kong Baptist University, Hong Kong, China

## Correspondence

Patricia M. Saco, Centre for Water Security and Environmental Sustainability and School of Engineering, The University of Newcastle, Callaghan 2308, Australia.

Email: [patricia.saco@newcastle.edu.au](mailto:patricia.saco@newcastle.edu.au)

## Funding information

Scientific and Technological Research Council of Turkey (TUBITAK), Grant/Award Numbers: grant 118C329, 118C329; Australian Research Council, Grant/Award Numbers: DP140104178, FT140100610; University of Newcastle Postgraduate Research Scholarship (UNRSC)

## Abstract

Topography affects the intensity and spatial distribution of precipitation due to orographic lifting mechanisms and, in turn, influences the prevailing climate and vegetation distribution. Previous modelling studies on the impact of orographic precipitation on landform evolution have considered bare soil conditions. However, research on the effect of changes in precipitation regimes induced by elevation gradients (particularly in aspect-controlled semi-arid ecosystems) on landform patterns, trying to understand feedbacks and consequences for coevolving vegetation, has been limited. In this study, the Channel–Hillslope Integrated Landscape Development (CHILD) landscape evolution model coupled with the vegetation dynamics Bucket Grassland Model (BGM) is used to analyse the coevolution of semi-arid landform–vegetation ecosystems. The CHILD+BGM model is run under different combinations of precipitation and solar radiation settings. Three precipitation settings, including uniform, elevation control, and orographic control on precipitation, are considered in combination with spatially uniform and spatially varied radiation settings. Based on the results, elevation control, aspect, and drainage network are identified as the major drivers of the distribution of vegetation cover on the landscapes. Further, the combination of orographic precipitation and spatially varied solar radiation created the highest asymmetry in the landscape and divide migration due to the emergence of gentler slopes on the windward than the leeward sides of the domain. The modelling outcomes from this study indicate that aspect control of solar radiation in combination with orographic precipitation plays a key role in the generation of topographic asymmetry in semi-arid ecosystems.

## KEYWORDS

CHILD+BGM, landscape evolution, orographic precipitation, semi-arid ecosystems, topographic asymmetry, vegetation

## 1 | INTRODUCTION

Precipitation patterns in mountain ranges are strongly controlled by orographic lifting mechanisms (Anders et al., 2008; Houze, 2012). The phenomenon of orographic precipitation is usually more pronounced in mountain ranges at mid-latitudes, and where the prevailing winds are perpendicular to the mountains (Chaboureaud, 2008; Colberg & Anders, 2014; Kirshbaum & Smith, 2008; Minder et al., 2010;

Roe, 2005; Roe & Montgomery, 2002; Roe et al., 2003; Shi & Durran, 2015). Many semi-arid regions across the world are highly dependent on freshwater supply from mountains, as a large proportion of the available runoff is produced in high-elevation areas (Scaff et al., 2017; Viviroli et al., 2007). Therefore, understanding the influence of precipitation–topography relationships in semi-arid ecosystems is critical for the analysis of the sensitivity of landscapes to changes in climate and vegetation cover.

This is an open access article under the terms of the [Creative Commons Attribution](https://creativecommons.org/licenses/by/4.0/) License, which permits use, distribution and reproduction in any medium, provided the original work is properly cited.

© 2022 The Authors. *Earth Surface Processes and Landforms* published by John Wiley & Sons Ltd.

The effect of orographic precipitation leads to a wetter climate that prevails on the windward side of a mountain flank compared to that on the leeward side, as the latter receives less precipitation. Elevation also controls precipitation and enhances differences in microclimatic conditions, as mean annual precipitation rates tend to increase with elevation (Anders et al., 2006; Colberg & Anders, 2014; Garreaud et al., 2016; Roe & Montgomery, 2002; Roe et al., 2003). Many researchers have investigated the relationship between rainfall and elevation across different sites worldwide (see e.g. Guan et al., 2005; Luce et al., 2013; Murata et al., 2007; Scaff et al., 2017). Guan et al. (2005) found that elevation is the major factor affecting precipitation distribution during winter months, while in the monsoon season both elevation and aspect have impacts on the distribution of precipitation. Further, Murata et al. (2007) highlighted the importance of the interaction between large-scale circulation effects and topography in determining the spatial distribution of rainfall over the Meghala Hills, India. Similar findings were obtained in central Chile, where synoptic-scale disturbances are strongly related to orographic precipitation and zonal moisture fluxes (Garreaud et al., 2016; Scaff et al., 2017).

The impacts of orographic precipitation on earth surface processes and landscape evolution have been explored in previous studies using both observational data (Ferrier et al., 2013; Goren et al., 2014; Han et al., 2014) and numerical experiments (Gasparini et al., 2008; Roe & Montgomery, 2002; Whipple et al., 1999). Thiede et al. (2004) showed that orographic precipitation strongly influences erosion rates, affecting the long-term evolution of topography in the Himalayas. Similar findings were reported by Clift et al. (2008), who found a clear correlation between Himalayan denudation rates and orographic effects of the South Asian monsoon. Anders et al. (2008) and Han et al. (2015) found that river networks and elevation distribution are also affected by orographic precipitation. Numerical simulations conducted by Goren et al. (2014) investigated the effects of orographic controls on landform evolution under constant uplift and no vegetation cover, revealing that windward slopes are longer and gentler than the leeward ones due to the presence of enhanced erosion induced by higher runoff. A key aspect missing from these previous landscape evolution studies is, however, the effect of coevolving landform-vegetation patterns under orographic precipitation conditions, and their possible implications for landform asymmetry (Paik & Kim, 2021; Smith & Bookhagen, 2021; Zavala et al., 2020).

Vegetation plays a key role in landscape evolution, as it modulates geomorphic processes, such as erosion and sediment transport (Collins & Bras, 2008; Dietrich & Perron, 2006; Kirkby, 1995; Langbein & Schumm, 1958; Moglen & Parsons, 1998; Saco & Moreno-de las Heras, 2013; Willgoose, 2018; Yetemen, Istanbuluoglu, Flores-Cervantes, et al., 2015). Early work by Langbein and Schumm (1958) quantified the non-linear relationship between precipitation and sediment yield and found that vegetation and precipitation exert competing effects, as precipitation increases and vegetation inhibits erosion. Moglen and Parsons (1998) extended this study by developing empirical relationships among erosion, vegetation, and climate to investigate the influence of climate change on drainage density. Using these empirical relationships, they found that, as the climate becomes wetter, vegetation becomes denser, offsetting the increase in erosion rates that could potentially result from increased runoff. Further work incorporating the effect of vegetation into landscape evolution models (LEMs) has revealed an increase in

dynamic equilibrium slopes with increased vegetation cover, which is due to an increase in resistance to sediment transport and erosion (see e.g. Collins & Bras, 2008; Istanbuluoglu & Bras, 2005; Saco et al., 2007; Yetemen, Istanbuluoglu, Flores-Cervantes, et al., 2015; Yetemen, Saco, & Istanbuluoglu, 2019).

Several modelling studies (Bartman et al., 2018; Collins & Bras, 2008, 2010; Collins et al., 2004; Istanbuluoglu & Bras, 2005; Saco & Moreno-de las Heras, 2013; Saco et al., 2007; Yetemen, Istanbuluoglu, & Duvall, 2015; Yetemen, Istanbuluoglu, Flores-Cervantes, et al., 2015) have investigated the coevolution of vegetation and landforms under different climatic and anthropic conditions. Collins et al. (2004) and Istanbuluoglu and Bras (2005) coupled the Channel-Hillslope Integrated Landscape Development (CHILD) LEM with vegetation-erosion dynamics and found that the dynamic vegetation cover (in which rainfall and solar radiation drive vegetation growth and senescence) led to the formation of a highly dissected topography with a significantly lower relief than the landscape evolved under static vegetation (vegetation remains constant). The results from the model with coevolving vegetation-landforms were found to better resemble natural landscapes. Results from Collins and Bras (2008) using CHILD indicated the existence of differences in vegetation recovery, with vegetation growth rates for drier climates being slower than for wetter climates due to the effect of limited water availability. Yetemen, Istanbuluoglu, Flores-Cervantes, et al. (2015) also incorporated the effect of spatially varied solar radiation, improving the LEM framework developed by Istanbuluoglu and Bras (2005) and Collins and Bras (2010), and showed that solar radiation is a major driver of topographic asymmetry in semi-arid landforms.

The effect of spatial vegetation patterns is linked to the emergence of spatially heterogeneous patterns of erosion. For example, modelling studies using SIBERIA (Willgoose et al., 1991a,b) and LAPSUS LEMs (Schoorl et al., 2000, 2002) suggest that the presence of banded vegetation patterns on coevolving landforms is linked to the emergence of stepped microtopography, which is observed in many field sites (Bartman et al., 2018; Saco & Moreno-de las Heras, 2013; Saco et al., 2007). Another important example of heterogeneous vegetation patterns that could affect erosion patterns is due to aspect-controlled differences on opposing hillslopes that generate variations in water stress patterns across slopes, particularly in semi-arid regions across the globe (Bass et al., 2017; Gutiérrez-Jurado et al., 2013; Kumari et al., 2019, 2020; Pelletier & Swetnam, 2017; Pelletier et al., 2018; Regmi et al., 2019; Yetemen, Istanbuluoglu, Flores-Cervantes, et al., 2015; Zou et al., 2007). In the Northern Hemisphere, the dense vegetation cover on the north-facing slopes (NFS) provides more erosion resistance, which counteracts the erosive effect of runoff. On the other hand, south-facing slopes (SFS) with sparser vegetation are prone to higher erosion (Istanbuluoglu et al., 2008). Such aspect-controlled vegetation differences exert pronounced influences on landscape morphology and can lead to differences in the way landforms evolve over time (Carson & Kirkby, 1972; Istanbuluoglu et al., 2008; Kirkby et al., 1990; McMahon, 1998; Srivastava et al., 2021; Yetemen, Istanbuluoglu, Flores-Cervantes, et al., 2015).

Despite the significant progress that has been achieved in analysing the interactions between vegetation patterns and landforms, and their relation to hillslope aspect and climatic controls, the understanding of potential feedback mechanisms is still limited. For example, to date, all modelling studies of the effect of orographic

precipitation on landform evolution have considered bare soil conditions, and have not accounted for the effect of vegetation cover (e.g. Goren et al., 2014; Han et al., 2015; Zavala et al., 2020). The study conducted by Goren et al. (2014) with a LEM showed that the windward side is longer than the leeward side of the mountain because higher rainfall and higher erosion rates generate a gentler slope on the windward side. Further modelling work by Paik and Kim (2021) to understand topographic asymmetry showed that the windward side receives more rainfall and so produces more runoff and sediment yield than the leeward side. As a result, the channels on the windward side propagate upstream at a faster rate, compared to those on the leeward side, which leads to a downward peak migration and a steeper slope.

As mentioned in previous paragraphs, topographic asymmetry in these studies was triggered by variations in precipitation between the windward and leeward sides of the mountain under bare soil conditions. However, topographic asymmetry can also be affected by the presence of spatially heterogeneous vegetation cover. The complex relation between shear stress (which increases due to increased runoff) and vegetation protection on the windward and leeward sides of the mountain can potentially affect topographic asymmetry (Willgoose, 2018). This type of effect can only be modelled by incorporating an aspect-controlled vegetation framework into LEMs and enabling the coevolution of landforms and vegetation under the effect of orographic precipitation.

This study constitutes the first attempt to analyse the role of orographic precipitation on the coevolution of landforms and aspect-controlled vegetation patterns in semi-arid ecosystems. To achieve this goal, the CHILD LEM (Tucker et al., 2001) modelling framework coupled with a vegetation dynamics component is modified to account for the influence of orographic and elevation control on precipitation, as well as solar radiation patterns, on vegetation and landscape evolution.

## 2 | MODEL STRUCTURE

The CHILD LEM coupled with the vegetation dynamics component BGM (Bucket Grassland Model) (Istanbulluoglu et al., 2012), which explicitly simulates the evolution of above- and below-ground biomass, is used in this study. A detailed description of the geomorphic processes included in the LEM, the processes simulated in the vegetation dynamics module, and the equations used to capture the spatial patterns of rainfall forcing is provided in the following subsections.

### 2.1 | Geomorphic dynamics

Geomorphic processes included in the LEM are described below. The continuity equation for sediment fluxes is used to compute changes in elevation, and accounts for geomorphic processes such as uplift, hillslope diffusion, and fluvial erosion as follows (Tucker et al., 2001):

$$\frac{dz}{dt} = U - \nabla \cdot q_d - F \quad (1)$$

where  $z$  [L] is elevation and  $t$  [T] is time. The first term on the right,  $U$  [ $LT^{-1}$ ], is the uplift; the second term corresponds to the divergence

of volumetric sediment flux per unit width by hillslope diffusion,  $q_d$  [ $LT^{-1}$ ]; and the third term,  $F$  [ $LT^{-1}$ ], corresponds to the divergence of the fluvial sediment transport [limited by detachment capacity, see Equation (3)]. Hillslope diffusion  $q_d$  varies with slope (Roering et al., 1999) as follows:

$$q_d = \frac{K_d \nabla z}{1 - \left(\frac{|\nabla z|}{S_{cr}}\right)^2} \quad (2)$$

where  $K_d$  is diffusivity [ $L^2T^{-1}$ ] and  $S_{cr}$  is the critical hillslope gradient. The fluvial erosion function,  $F$ , is simulated as

$$F = \begin{cases} -\nabla q_f, & \text{where } D_c > q_f \\ -D_c, & \text{elsewhere} \end{cases} \quad (3)$$

where  $\nabla q_f$  represents net divergence of fluvial sediment flux per unit width [ $LT^{-1}$ ] and  $D_c$  is the detachment capacity [ $LT^{-1}$ ], which prescribes the maximum rate of local erosion.  $\tau_{eff}$  is approximated using the boundary shear stress ( $\tau_{bs}$ ) (detailed in the online Supporting Information) and scaled using the ratio of Manning's roughness coefficient of vegetation ( $n_v$ ) and bare soil ( $n_s$ ) as (Istanbulluoglu & Bras, 2005; Yetemen, Istanbulluoglu, Flores-Cervantes, et al., 2015):

$$\tau_{eff} = \tau_{bs} \left( \frac{n_s}{n_s + n_v} \right)^{3/2} \quad (4)$$

where  $n_v$  is represented as a power function of its reference vegetation cover fraction,  $V_R = 0.95$ , which has a roughness coefficient,  $n_{vR} = 0.5$  (Istanbulluoglu & Bras, 2005), as

$$n_v = n_{vR} \left( \frac{V}{V_R} \right)^\omega \quad (5)$$

where  $\omega$  is the parameter that quantifies the relation between vegetation roughness and surface vegetation cover fraction, which is computed using the BGM as described in the next subsection.

### 2.2 | Vegetation dynamics

The dynamics of the vegetation cover fraction is simulated using the single-layer BGM for a single plant functional type (i.e. grass). BGM simulates the ecohydrologic response of vegetation driven by precipitation pulses, using a single bucket with a vertically averaged soil moisture content in the root zone. The fractions of grass (live and dead) and bare soil in each cell are updated following every storm event using the procedure described below.

The net primary productivity (NPP) of grass biomass ( $g/m^2$ ) is calculated as a function of interstorm evapotranspiration ( $ET_d$ ) [ $LT^{-1}$ ] and water use efficiency (WUE) and then allocated to aboveground and belowground biomass compartments (Swenson & Waring, 2006), as follows:

$$NPP = 0.75 \cdot (1 - \mu) \cdot ET_d \cdot WUE \cdot \rho_w \cdot \omega \quad (6)$$

where  $\mu$  is the ratio of exchange of  $CO_2$  from daytime to night-time,  $\rho_w$  is the density of water, and  $\omega$  is a conversion factor of  $CO_2$  to dry

biomass (kg DM/kg CO<sub>2</sub>). The sum of aboveground and belowground grass biomass production at the ecosystem scale is linearly related to  $ET_a$  by using the  $WUE$  value (the ratio of biomass produced by the plants to the amount of water transpired by a plant).  $WUE$  (kg CO<sub>2</sub>/kg H<sub>2</sub>O) is obtained as (Farquhar et al., 1989):

$$WUE = \frac{p_a \left(1 - \frac{p_i}{p_a}\right)}{1.6\Delta e} \quad (7)$$

where  $p_a$  and  $p_i$  are the ambient and intercellular partial pressures of CO<sub>2</sub>, respectively and  $\Delta e$  is the change in the water vapour pressure inside the leaf and in the air, respectively.

Biomass (g DM m<sup>-2</sup>) decays following first-order reaction kinetics, which is regulated by water stress (Yetemen, Istanbuluoglu, Flores-Cervantes, et al., 2015). Two separate biomass states (compartments) are tracked: green aboveground ( $B_g$ ) and dead biomass ( $B_d$ ). Biomass components are modelled after Montaldo et al. (2005), as follows:

$$\frac{dB_g}{dt} = NPP \cdot a_c - k_g B_g - k_i B_g \xi_s \quad (8)$$

$$\frac{dB_d}{dt} = k_g B_d - k_h B_d \xi_d \quad (9)$$

where  $a_c$  is the allocation coefficient,  $k_g$  and  $k_h$  represent decay coefficients for green and dead biomass, respectively,  $k_i$  is the coefficient for drought-induced foliage loss,  $\xi_d$  is a coefficient for climate influence on dead biomass, and  $\xi_s$  is a water stress function for green biomass (detailed in the online Supporting Information).

The vegetation cover fraction,  $V_t$  [-], for total biomass is computed using an exponential function, as proposed by Lee (1992):

$$V_t = [1 - \exp(-0.75 \cdot LAI_t)] \quad (10)$$

## 2.3 | Rainfall input

As mentioned in the Introduction, the goal of this study is to investigate the impact of rainfall patterns induced by elevation and orographic effects on the coevolution of landform and vegetation. This section describes the equations incorporated as input into the coupled CHILD+BGM framework to capture these rainfall distribution patterns.

A modified version of a Poisson rectangular pulse rainfall model is used in CHILD to generate the stochastic rainfall forcing (Eagleson, 1978). Every storm event is considered to have three essential characteristics: storm intensity,  $p$  [LT<sup>-1</sup>]; storm duration,  $T_r$  [T]; and interstorm period,  $T_b$  [T]. Every storm has a constant rainfall intensity, which is followed by an interstorm period. One-parameter exponential distributions are used to generate storm and interstorm period (Eagleson, 1978), whereas a two-parameter gamma distribution is used to generate the storm intensity to represent the dependence between intensity and duration (Ivanov et al., 2007). The mean values of the storm characteristics ( $\bar{p}$ ,  $\bar{T}_b$ , and  $\bar{T}_r$ ) are estimated as a function of mean annual precipitation (MAP) based on empirical relations developed for the semi-arid southwestern United States (Small, 2005).

In order to incorporate the elevation and orographic effects, the spatial precipitation pattern is computed as a function of elevation, and spatial location on the landscape. The precipitation amount for each pixel is computed using a relation that varies linearly with elevation, and that considers its possible location in windward and leeward flanks of the mountain. Linear models for orographic control on precipitation are simple and have been used extensively in the literature (Nearing et al., 2015; Osborn, 1984; Wainwright, 2005). Precipitation  $P_z$  at a given cell with elevation  $Z_i$  is obtained as

$$P_z = P \left[ \left(1 + \frac{Z_i - Z_o}{Z_{max} - Z_o}\right) P_{wind} + AspF \left(\frac{Z_{max} - Z_i}{Z_{max} - Z_o}\right) P_{lee} \right] \quad (11)$$

where  $P$  is the precipitation at  $Z_o$  and  $Z_o$  is the lowest elevation [m].  $Z_i$  represents the cell elevation [m] and  $Z_{max}$  is the maximum elevation [m].  $P_{wind}$  [m<sup>-1</sup>] is the windward orographic precipitation parameter and  $P_{lee}$  [m<sup>-1</sup>] is the leeward orographic precipitation parameter. The precipitation is scaled linearly as a function of the elevation and adjusted to account for the orographic position using the windward and leeward parameters ( $P_{wind} = 0.5$  and  $P_{lee} = 0.15$ ), and the  $AspF$  factor [-] that defines on which side of the mountain range the cell is (i.e. windward or leeward).  $AspF$  is assigned after comparing the downstream direction of each cell with the wind direction. The cell is assigned as windward if the downstream direction is opposing the wind direction (the angle between the two directional vectors is  $>90^\circ$  and  $<270^\circ$ ), or leeward if the downstream direction is aligned with the wind direction (the angle is  $\leq 90^\circ$  or  $\geq 270^\circ$ ):

$$AspF = \begin{cases} 0, & \text{windward} \\ -1, & \text{leeward} \end{cases} \quad (12)$$

Figure S1 (in the online Supporting Information) illustrates the distribution of precipitation for the simple domain with elevations depicted in Figure S1a, obtained from Equation (11) considering only uniform precipitation (Figure S1b), elevation effects (Figure S1c), in which  $AspF = 0$  in all cells, and considering both elevation and orography effects (Figure S1d).

## 3 | METHODOLOGY

The role of different precipitation settings on coevolving landforms-vegetation patterns is investigated using the CHILD+BGM model. The model is parametrized based on work from previous studies (Yetemen, Istanbuluoglu, & Duvall, 2015; Yetemen, Istanbuluoglu, Flores-Cervantes, et al., 2015) that calibrated the model and validated the results (using soil moisture, runoff, and satellite-based LAI data) for a site in the Sevilleta National Wildlife Refuge (SNWR) in central New Mexico. A brief overview of the synthetic domain and the design of the numerical experiments used in this study is presented below.

### 3.1 | Synthetic domain

Figure 1 shows the two-sided synthetic domain used in the CHILD+BGM LEM to explore the effect of different rainfall settings on the

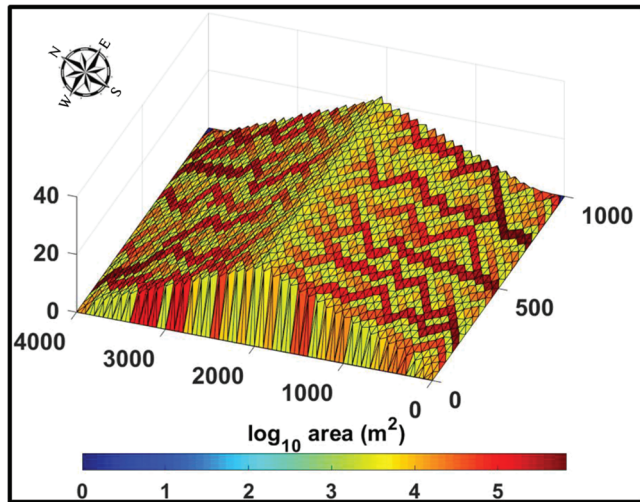


**FIGURE 1** Two-sided synthetic domain (showing contributing drainage area in  $\text{m}^2$ ) used in the design of the numerical experiments in the current study.

coevolution vegetation and landforms. The CHILD model is run on a  $1000 \times 4000$  m triangulated irregular network domain constructed using 50 m regularly spaced nodes such that the fluxes of surface runoff and sediment are permitted through the two open-boundary downslope edges. As shown in Figure S1, the elevation is highest at 2000 m. All model simulations are run for 800 000 years and driven by an uplift rate of  $U = 0.25$  mm/year, so that the simulated landscapes attain dynamic equilibrium between erosion ( $E$ ) and uplift ( $E \cong U$ ). The uplift rate used in this study is within the range of the long-term ( $\sim 640$  ka) average values reported in the literature for the region (Bierman et al., 2005; Clapp et al., 2001; Dethier, 2001). Previous modelling studies have also utilized such a range of uplift values in the same study region (Srivastava et al., 2021; Yetemen, Istanbuluoglu, & Duvall, 2015; Yetemen, Istanbuluoglu, Flores-Cervantes, et al., 2015; Yetemen et al., 2019).

The results for the last 100-year period corresponding to elevation, erosion, and vegetation cover fraction ( $V_t$ ) in each grid cell are used to examine differences in landform, erosion, and vegetation patterns resulting from the different precipitation and radiation settings described next.

### 3.2 | Numerical experimental settings

Several simulations to understand the combined role of solar radiation and different precipitation settings on the coevolution of vegetation patterns and semi-arid landforms are conducted using CHILD+BGM on the synthetic domain shown in Figure 1. In order to elucidate the role of solar radiation on the spatial distribution of vegetation cover, two different scenarios are used: (i) (spatially) uniform radiation and (ii) slope control on radiation. For the first case, solar radiation is assumed to be uniform in space and estimated as the value corresponding to a flat surface for the latitudinal location of the study site. This spatially uniform value is varied in time as a function of day of the year. In the second case (slope control), solar radiation for each cell (and for each day) is computed as a function of aspect and slope gradient throughout the domain.

In order to investigate the role of different precipitation settings on the coevolving vegetation–landform patterns, three different scenarios are designed: (i) (spatially) uniform precipitation, (ii) elevation control precipitation, and (iii) orographic precipitation. Figure 2 illustrates the spatial distribution of precipitation over the synthetic domain for the three scenarios, for a given storm event. In the uniform precipitation case, all grid cells receive the same amount of precipitation (Figure 2a). In the elevation-controlled case, precipitation varies as a function of elevation (Figure 2b) and is computed using Equation (11) with the parameter  $AspF = 0$ .

Finally, the distribution of the precipitation for the case considering the orographic rainfall shadow effect on the leeward side (orographic control) is shown in Figure 2c and computed using Equations (11) and (12). Precipitation increases by approximately 1.75 times the lower values in the boundary edge to the peak elevations on the leeward side [according to Equations (11) and (12). On the windward side of the domain, the top precipitation value represents only a 1.5 times increase with respect to the lower values on the boundary edge (the distribution of precipitation for a simplified domain is illustrated in Figure S1). Similar linear orographic precipitation models, which provide an idealized representation of the relationship between precipitation and topography, have successfully been used in many climatological studies (Anders et al., 2006; Lundquist et al., 2010; Minder et al., 2010; Smith, 2003; Smith & Barstad, 2004). Several examples of real-world landscapes can be found (Malby et al., 2007; Rata et al., 2020; Wainwright, 2005; Webb et al., 2003) that show increases in precipitation of 100 mm over short distances with elevation rises of  $\sim 100$  m, as selected as input for our modelling framework. For instance, Webb et al. (2003) reported the relation between elevation and annual precipitation in Nevada, such that a precipitation rise of approximately 80–100 mm was observed for  $\sim 100$  m increase in elevation. Similar findings were also observed by Wainwright (2005) for their study conducted in Jornada Experimental Range, New Mexico. Furthermore, Malby et al. (2007), in their observations in the Lake District region, northwest England, reported an increase in precipitation from  $\sim 200$  mm/year at low elevations ( $\sim 20$  m) to 300 mm/year at high elevations ( $\sim 120$  m). In another real-world site, Cheliff watershed in northwestern Algeria, Rata et al. (2020) indicated a precipitation increase of 250–350 mm/year over  $\sim 100$  m rise in elevation.

In total, six different scenarios are designed using a combination of the two different solar radiation conditions and the three different precipitation settings described above. In order to quantify the independent effect of different precipitation patterns on landforms and vegetation, a set of experiments with uniform solar radiation are run using (a) uniform, (b) elevation control, and (c) orographic precipitation (see Table S1 in the online Supporting Information). A set of three experiments are also conducted with the combined effect of slope control on radiation and the three precipitation patterns: (d) uniform, (e) elevation control, and (f) orographic precipitation (Table S1). The experiment with slope control on radiation and uniform precipitation is designed to single out the role of aspect on the coevolving landscape. The results for the six scenarios are described in the following section.

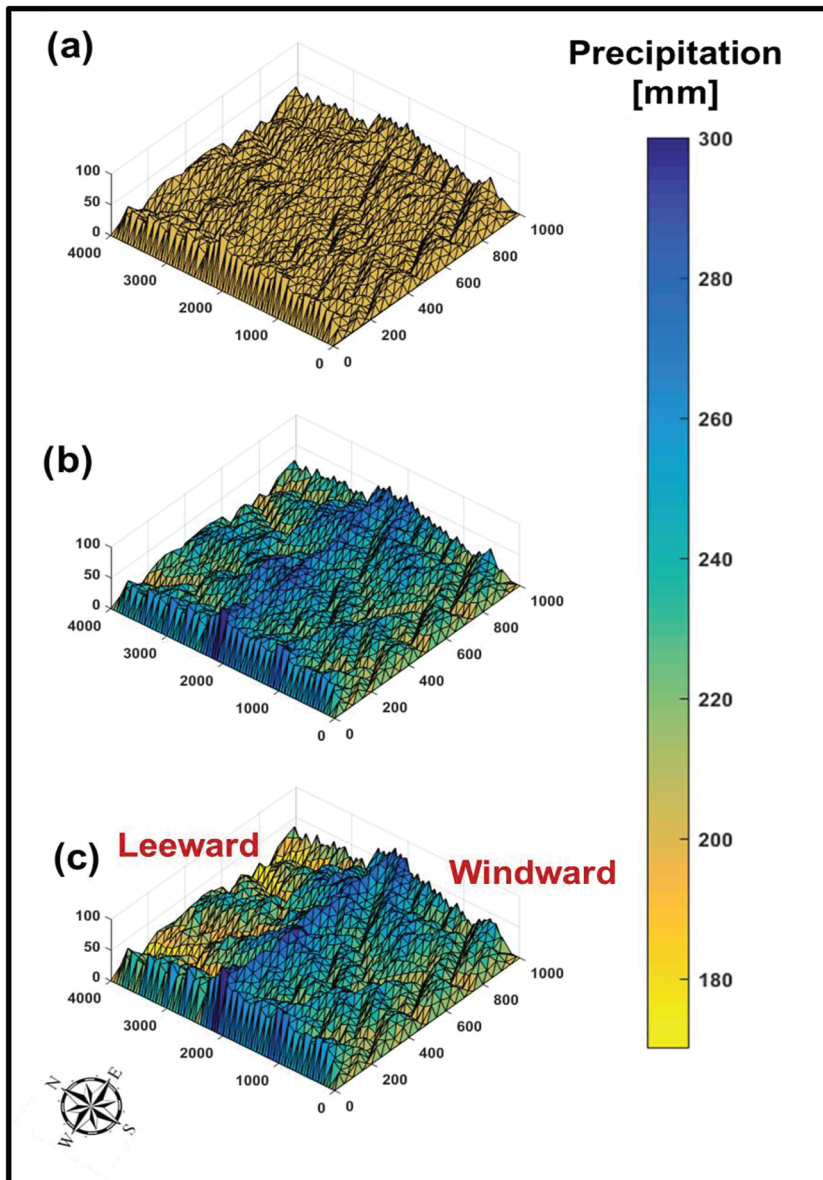


**FIGURE 2** Schematic illustrating the spatial distribution of precipitation on top of the topographic domain, at a given time step, for the three different settings: (a) uniform precipitation; (b) elevation control precipitation; and (c) orographic precipitation. Precipitation values are represented by colours. The vertical axis represents elevation in metres.

## 4 | RESULTS

### 4.1 | Influence of precipitation and radiation patterns on the spatial distribution of vegetation

The spatial patterns obtained for the mean values of vegetation cover (for the last 100 years of simulation) for the six scenarios are displayed in Figure 3 (the corresponding three-dimensional plots are provided in Figure S2 of the online Supporting Information). The simulated mean vegetation cover pattern for the uniform solar radiation and uniform precipitation scenario is shown in Figure 3a. The higher values of the vegetation cover fraction, with a maximum of 0.28, occur in the channels (higher contributing areas). This highlights a dominant network control on vegetation patterns for this scenario, since the incoming solar radiation and precipitation are uniform and the only observed spatial variability in vegetation distribution is due to the enhanced soil moisture in areas of flow concentration.

The spatial pattern of the mean simulated vegetation cover fraction for the uniform solar radiation setting, in combination with elevation control precipitation, is shown in Figure 3b. Higher vegetation

cover (darker green pixels) is mostly concentrated towards the middle of the domain, where elevations are higher (~1500–2500 m). This highlights the dominant control of elevation on the vegetation cover pattern, driving higher precipitation rates in these areas. This is also reflected in the higher amount of vegetation cover fraction (with respect to that of the previous case) which, for this scenario, reaches a value of ~0.3 at high elevations. Areas with lower elevations that receive comparatively less precipitation on both sides of the domain have a lower vegetation cover (~0.05). The effect of elevation control is very strong and almost completely counteracts the effect of the drainage network.

Figure 3c shows the spatial pattern of the mean vegetation cover fraction for simulations with orographic precipitation and uniform solar radiation inputs. In this case, the amount of vegetation cover is higher on the windward side of the domain (approximately 0–2000 m in the northing direction) than on the leeward side (approximately 2000–4000 m), as rainfall is higher on the windward side due to the orographic effect. As in the previous case, the effect of increased vegetation at higher elevations (with higher precipitation) towards the middle of the domain in the northing direction also characterizes this pattern.

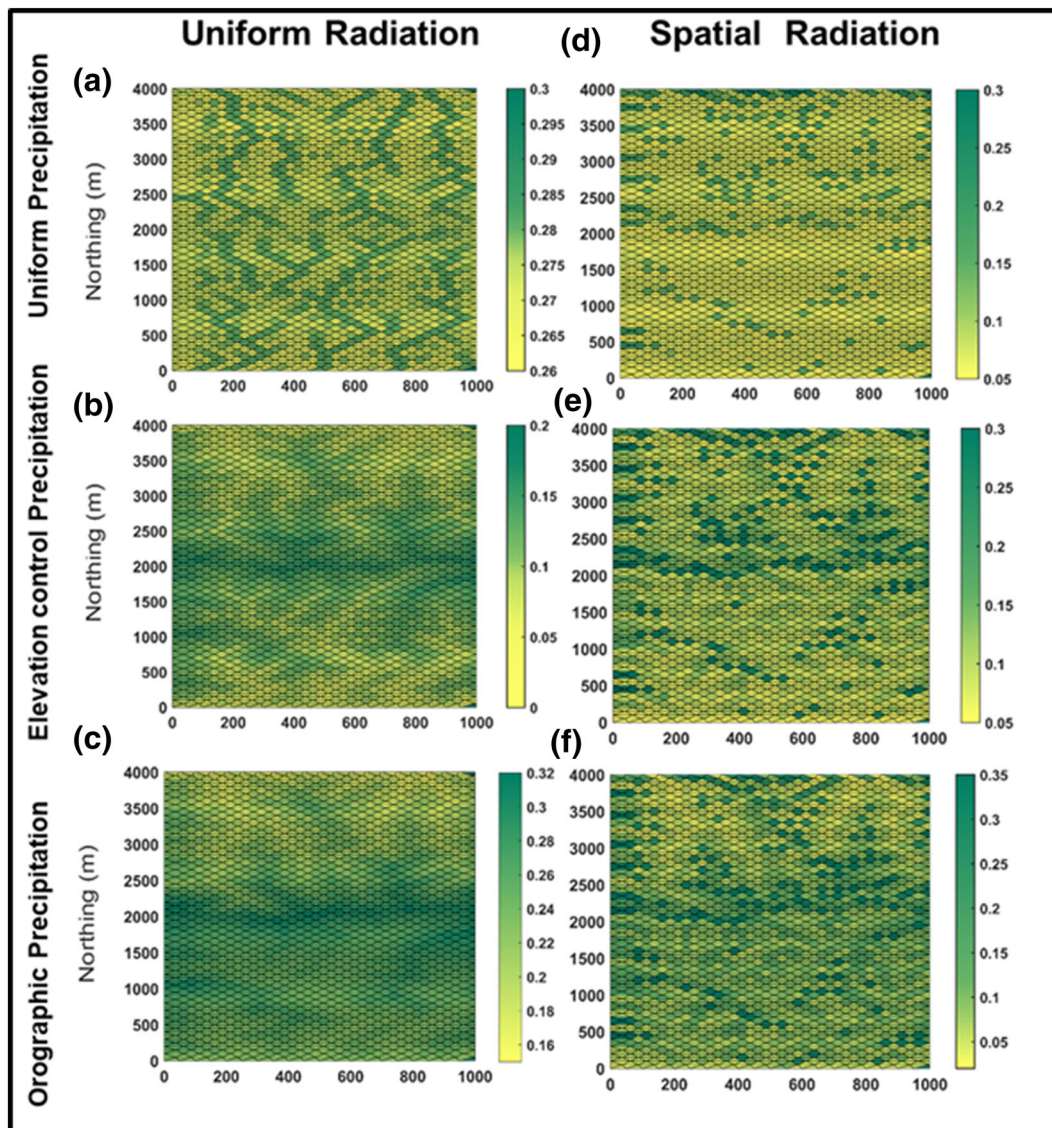


**FIGURE 3** Spatial patterns of the simulated vegetation cover fraction (mean values over the last 100-year period) for the different precipitation and solar radiation scenarios. The left panel (first column) shows the results for the uniform solar radiation scenario for (a) uniform precipitation, (b) elevation control precipitation, and (c) orographic precipitation. The right panel (second column) shows the spatially varied solar radiation scenario for the three precipitation patterns. Note that the range of values (colour bands) varies for different scenarios.

The resulting mean vegetation cover pattern for the case of spatially varied solar radiation in combination with uniform precipitation is presented in Figure 3d. A higher range of vegetation cover fraction values ( $\sim 0.05$ – $0.3$ ) is obtained in this case when compared to those for the uniform solar radiation scenario. The distinct differences between the patterns shown in Figures 3a and d suggest that the spatial variability of solar radiation and its associated aspect-driven effects dominate the vegetation response (the aspect distribution is shown in Figure S3 of the online Supporting Information). A similar spatial pattern is obtained for the case of spatially varied solar radiation combined with elevation control precipitation (Figure 3e). The aspect control of solar radiation is reflected in the presence of a higher vegetation cover fraction on NFS, but in this case the increase in vegetation cover fraction is more pronounced at higher elevations as is evident from Figures 3e and d.

Finally, Figure 3f shows the spatial pattern of simulated vegetation cover fraction for the spatially varied solar radiation under the orographic precipitation input. This pattern resembles the same

features of the two previous cases (Figures 3e and d) but with the additional effect induced by increased precipitation on the windward mountain flank which enhances vegetation compared with the leeward flank. The aspect control of solar radiation is also evident, with NFS on the windward side having higher vegetation cover fraction than their leeward counterparts due to the effect of orographic precipitation.

The role of aspect and elevation on vegetation cover patterns is further investigated by classifying all pixels in the domain into four cardinal direction categories and analysing the results for each category (or aspect). Each pixel is classified into four cardinal directions measured clockwise: North =  $315^\circ$ – $360^\circ$  and  $0^\circ$ – $45^\circ$ ; East =  $45^\circ$ – $135^\circ$ ; South =  $135^\circ$ – $225^\circ$ ; and West =  $225^\circ$ – $315^\circ$ . Figure 4 shows scatterplots of the mean total vegetation cover fraction as a function of elevation for the three different precipitation distributions (i.e. uniform, elevation control, and orographic) considering its aspect.

The mean total vegetation cover as a function of elevation for NFS and SFS for the scenario with uniform precipitation is presented

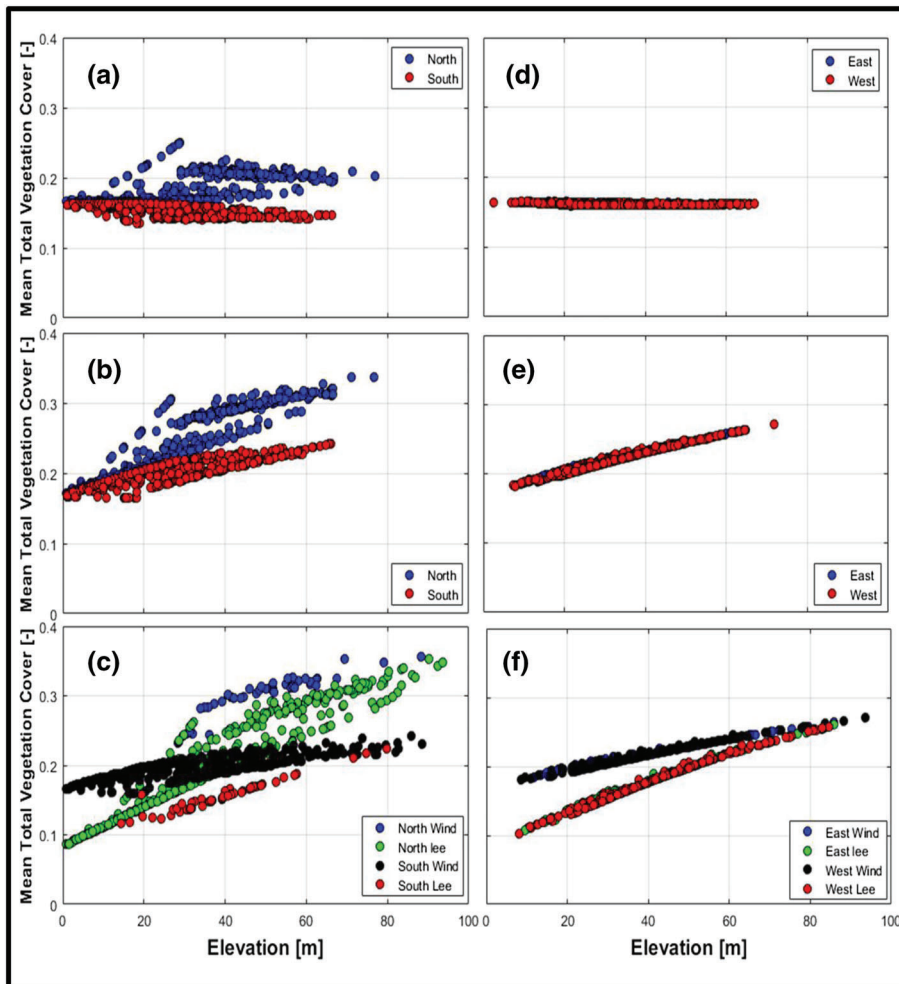


**FIGURE 4** Simulated mean total vegetation cover as a function of elevation on NFS and SFS (first panel) and EFS and WFS (second panel) for different precipitation settings: (a) uniform precipitation, (b) elevation control precipitation, and (c) orographic precipitation. NFS and SFS on the windward side are represented by ‘north wind’ and ‘south wind’, respectively. While NFS and SFS on the leeward side of the synthetic domain are illustrated by ‘north Lee’ and ‘south Lee’, respectively. EFS and WFS on the windward side are represented by ‘east wind’ and ‘west wind’, respectively. While EFS and WFS on the leeward side of the synthetic domain are illustrated by ‘east Lee’ and ‘west Lee’, respectively.

in Figure 4a. Vegetation cover in this case does not change significantly with elevation as precipitation is uniformly distributed. The trends observed as a function of elevation in this figure are produced by the effect of slope steepness. As a result of differences in insolation, NFS (which have lower evapotranspiration) have a denser canopy than SFS. Upper hillslope areas are usually steeper (as will be discussed in more detail in later sections), which affects insolation. Steep NFS have lower insolation than gentle slopes, while steep SFS have higher insolation than gentle ones, which explains the trends observed for higher elevations, as areas with higher insolation have higher evaporation and lower soil moisture and therefore a reduced vegetation cover. Figure 4b shows the mean vegetation cover as a function of elevation under the combined effect of spatially varied radiation and elevation control on precipitation. Like in the previous scenario, NFS have higher vegetation cover than SFS, but in this case, vegetation cover increases as a function of elevation. Mean vegetation cover ranges from 0.18 to 0.35 for NFS, while it ranges from 0.18 to 0.24 for SFS.

Differences in mean vegetation cover fraction as a function of elevation for NFS and SFS on the windward and leeward sides of the domain obtained for the case of orographic precipitation and spatially varied radiation are shown in Figure 4c. The highest values of vegetation cover fraction ( $\sim 0.38$ ) are found in cells with a north windward position. These values are always higher than those for cells with the same elevation but located in the north leeward, south windward, and south leeward positions. The relationship between the vegetation

cover and elevation for this scenario is more complex, due to the combined (and sometimes competing) effects of solar radiation and precipitation, which vary differently in the windward and leeward flanks. As seen in Figure 4c, the lower vegetation cover fraction observed for SFS is found on the leeward side and is due to the combination of soil moisture stress induced by solar radiation and the orographic effect. However, the spatial pattern has the lowest vegetation cover on NFS on the leeward side, as it is here where the lowest elevations are found. These slopes receive the lowest amount of rainfall due to the combination of low elevation and orographic shadow effect. It is also worth noting that at higher elevations ( $> \sim 30$  m), NFS on the leeward side have higher vegetation cover than SFS on the windward side of the domain, because precipitation at higher elevations is similar on both sides, so the effect of solar radiation becomes dominant. These results suggest that vegetation patterns are strongly affected by the interplay between rainfall and solar radiation patterns.

Figure 4d shows the mean vegetation cover as a function of elevation for east-facing slopes (EFS) and west-facing slopes (WFS) for the uniform precipitation and spatially varied solar radiation setting. EFS and WFS have a similar amount of vegetation cover fraction ( $\sim 0.18$ ) across the entire elevation range, as the role of aspect is not significant on EFS and WFS and their value of vegetation cover fraction is similar to that for a flat surface. Figure 4e shows the mean vegetation cover fraction as a function of elevation for the elevation control precipitation and spatially varied solar radiation setting, which reflects the increase in rainfall with elevation, but, again, shows no



differences in vegetation cover between EFS and WFS. Figure 4f shows that when considering the effect of orographic precipitation, EFS and WFS on the windward side can support higher vegetation cover than those on the leeward side due to the precipitation shadow effect.

#### 4.2 | Influence of different precipitation and solar radiation settings on divide migration

Figure 5 displays the development of topographic asymmetry over the entire simulation period for all the study cases by showing pixels that migrate from the windward side of the domain towards the leeward side of the domain. For the case with uniform precipitation and uniform radiation (Figure 5a), no divide migration is visible, as an almost negligible number of pixels shift. On the other hand, when precipitation is uniform but solar radiation varies spatially due to the

effect of aspect (Figure 5d), it can be seen that a few pixels tend to migrate. This is due to aspect-related differences in vegetation distribution. Figures 5b and e show a similar pattern for elevation control precipitation but with a larger number of pixels shifting. In this case, the role of aspect (Figure 5e) induces a higher divide migration than that for the case of uniform solar radiation (Figure 5b). Figures 5c and f show the significant shift in the divide away from the centre of the domain towards the leeward side for the orographic precipitation case, particularly when aspect-controlled solar radiation is considered (Figure 5f).

In order to further explore the emerging topographic asymmetry that leads to divide migration results described above (Figure 5), the elevation maps and slope–area diagrams for both sides of the domains are displayed in Figures 6 and 7, respectively. In Figure 7, the green dots display the mean slopes for all cells in the frontal portion of the domain (up to the divide), while the yellow dots display the mean slopes for the back portion of the domain. The two scenarios

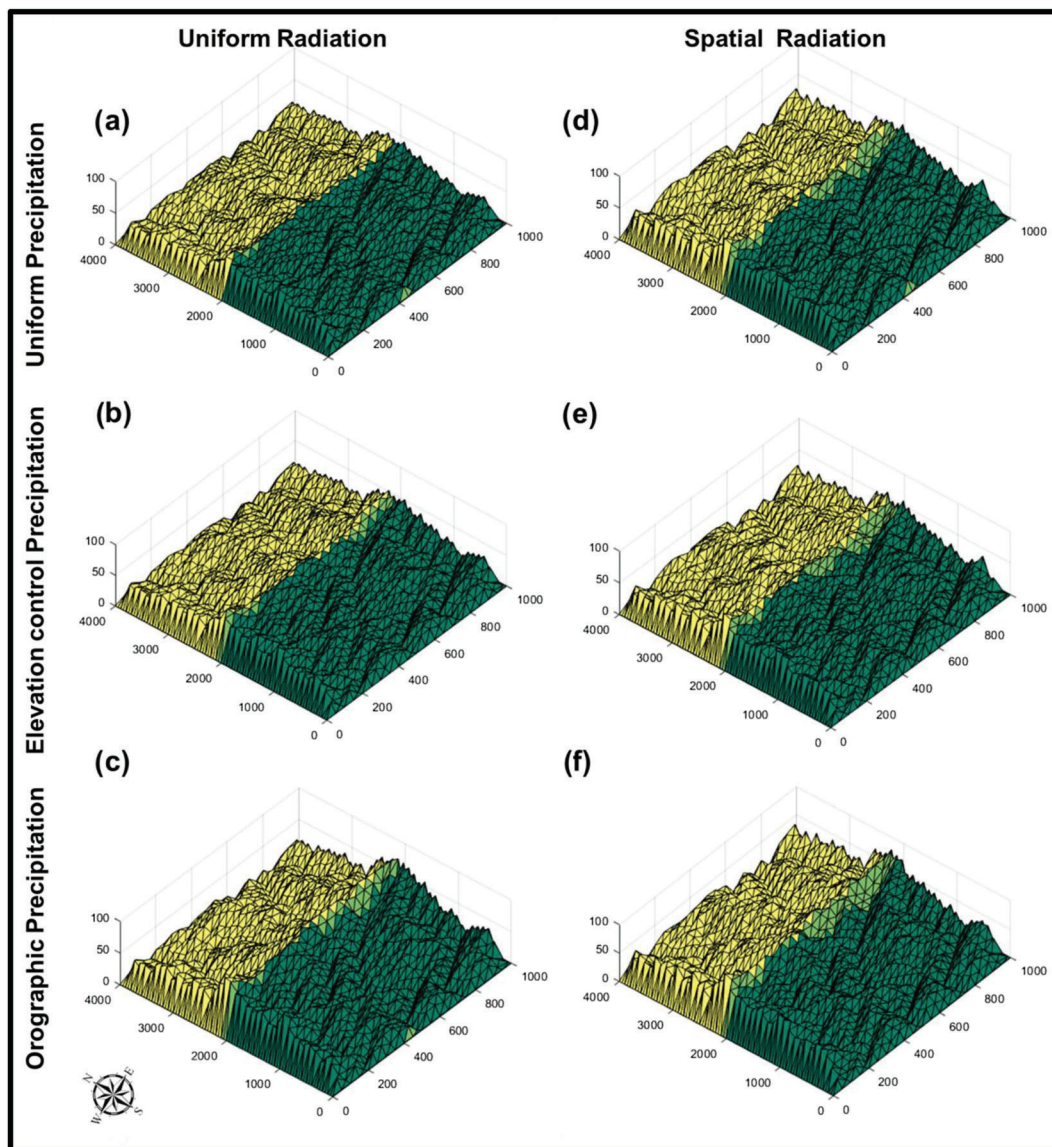


**FIGURE 5** Results showing divide migration for the different precipitation and solar radiation cases. The left column of the diagram shows the uniform solar radiation cases for (a) uniform precipitation, (b) elevation control precipitation, and (c) orographic precipitation. The right column of the diagram shows the spatial radiation cases for (d) uniform precipitation, (e) elevation control precipitation, and (f) orographic precipitation. Green represents the windward side of the domain and yellow represents the leeward side with respect to orographic precipitation. Finally, light green indicates pixels undergoing migration.

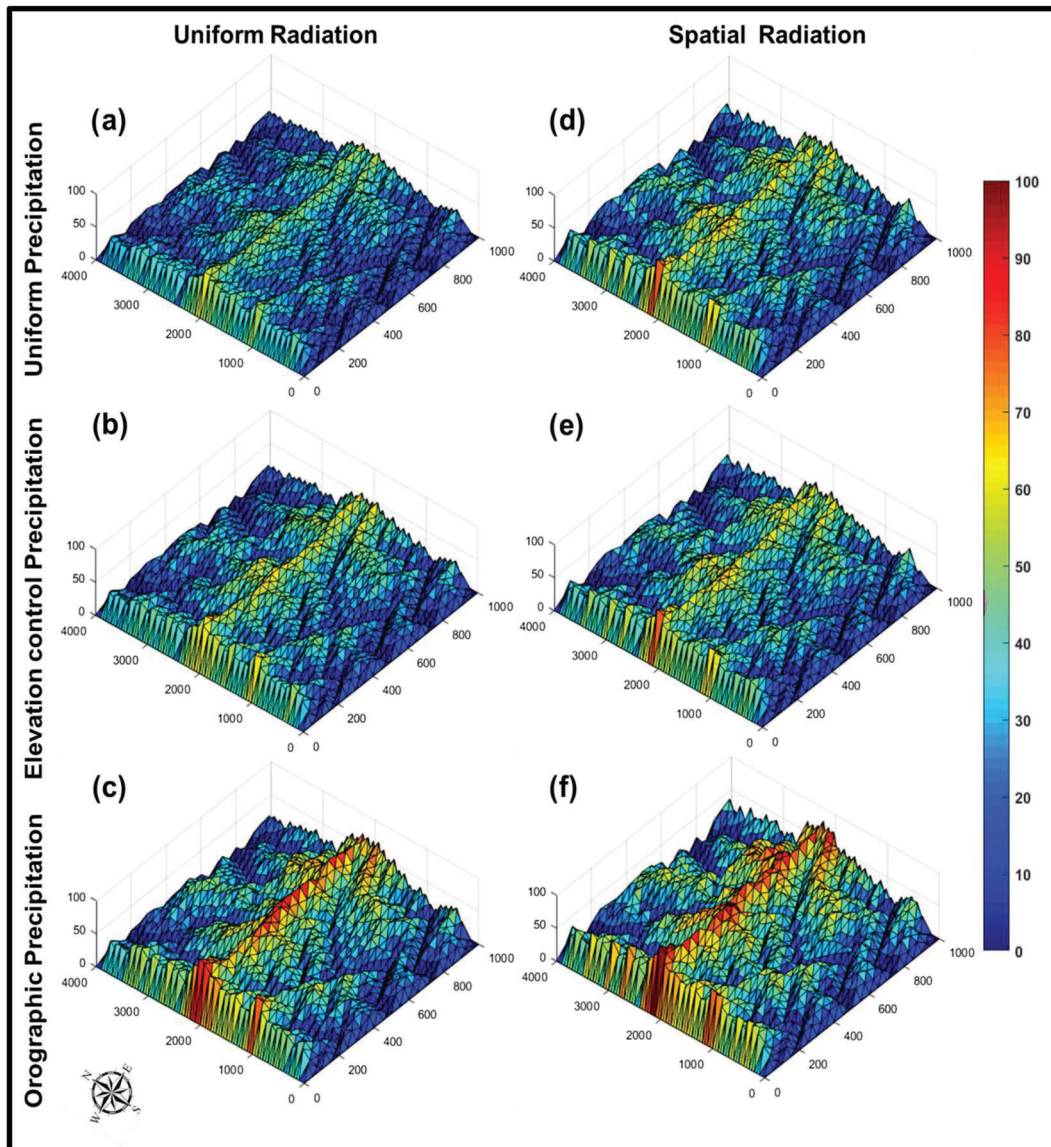


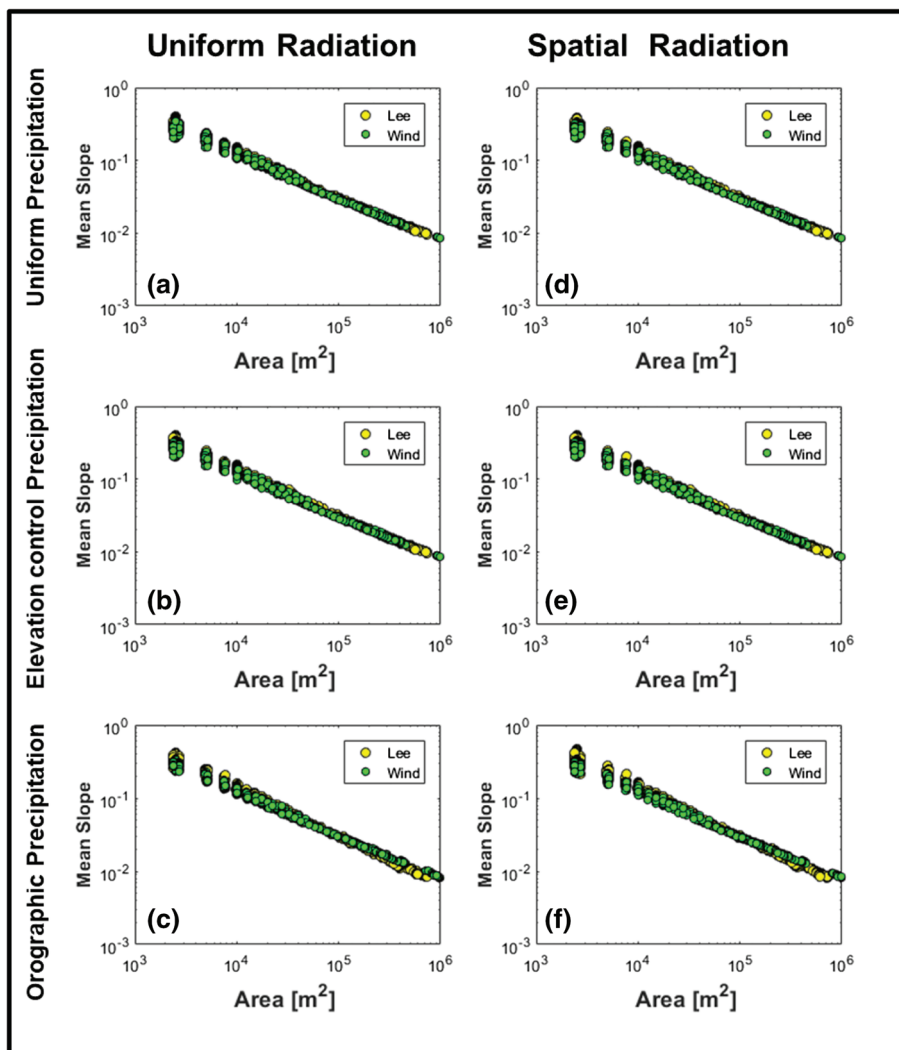
**FIGURE 6** Three-dimensional views of modelled elevation map from the CHILD model for different precipitation and solar radiation cases. The elevation map is plotted on modelled topography, where the left column of the diagram shows the uniform solar radiation cases for (a) uniform precipitation, (b) elevation control precipitation, and (c) orographic precipitation. The right column of the diagram shows the spatially varied solar radiation cases for (d) uniform precipitation, (e) elevation control precipitation, and (f) orographic precipitation.

corresponding to uniform and elevation control on precipitation and uniform radiation which, as mentioned above, display almost no divide migration are characterized by negligible differences in mean slopes between both sides of the domain (Figures 7a and b). Though there are very small differences in the elevation between the uniform precipitation and elevation control precipitation cases with spatially varied radiation (Figures 6d and e), Figures 7d and e show some subtle differences in slope, with those on the back side being slightly steeper than those on the frontal flank due to the effect of aspect that is enhanced by elevation control leading to higher vegetation (Figure 3b) and therefore more resistance to erosion on the back flank of the domain (note that this case displays a higher number of migrating pixels than the uniform radiation case in Figure 5).

When orographic precipitation is considered (Figures 6c and f), the simulated elevations at the divide tend to be higher than those from the other precipitation scenarios, due to differences in the vegetation protection on windward and leeward sides of the domain. An

interesting result captured in Figures 7c and f is that the slopes of the leeward face are steeper than the windward slopes for locations with low contributing areas, but the opposite is found for larger contributing areas (differences are less significant but highlighted by the logarithmic nature of this plot). This effect is slightly more pronounced for the case that accounts for differences in aspect (variable radiation), which can be explained by the fact that the cells with low contributing areas are generally located in the upper portions of the catchment. The discharge is smaller in the back or leeward side (see also Figure 9), so dynamic equilibrium conditions (in which erosion is the same everywhere in the catchment) can only be achieved if areas on the leeward side that have less discharge for the same contributing area (and similar vegetation) are steeper than areas with the same contributing area but higher discharge (in the front or windward side). On the other hand, high contributing areas are mostly located in areas at lower elevations, and it is in these locations that vegetation is significantly different on both flanks, with much higher vegetation cover fraction on the

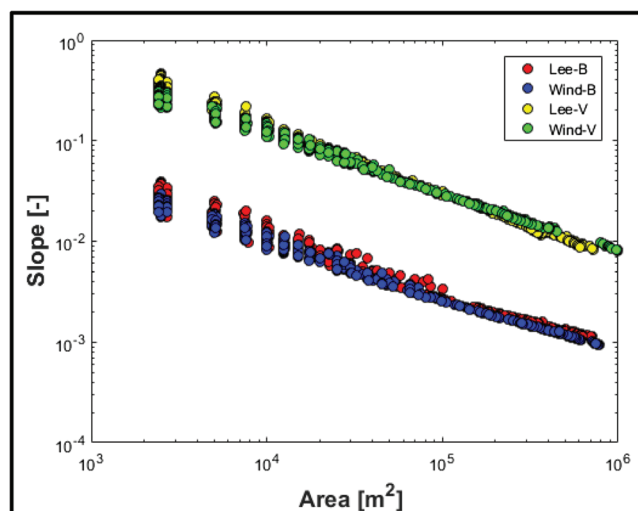
**FIGURE 7** Slope–area relationship of the modelled landscapes for different precipitation and solar radiation cases. The left column of the diagram shows the uniform solar radiation cases for (a) uniform precipitation, (b) elevation control precipitation, and (c) orographic precipitation. The right column of the diagram shows the spatially varied solar radiation cases for (d) uniform precipitation, (e) elevation control precipitation, and (f) orographic precipitation.



windward side due to the rainshadow effect (as shown in Figures 3c and f, and Figure 4c). This leads to steeper hillslopes on the windward side that is more protected from erosion. In this case, the protective effect of vegetation cover becomes dominant over the erosive effect of the increasing runoff driven by higher contributing areas. These findings are in agreement with results from Yetemen et al. (2019) for the case of a single slope undergoing changes in climate over time.

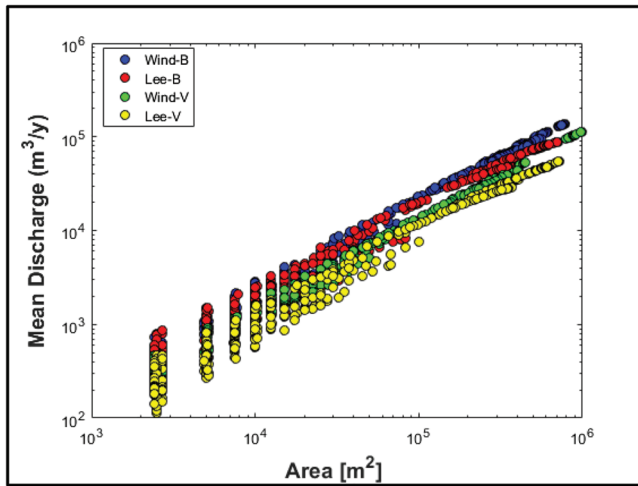
Simulations for bare soil conditions are also performed in order to compare the trends in slope changes for windward and leeward locations and divide migration to those discussed in previous modelling studies (Goren et al., 2014; Han et al., 2015). It is interesting to note that the simulations for bare soil conditions, using spatially varied radiation and orographic precipitation settings, displayed lower divide migration than the simulations using the same scenario but including dynamic vegetation (see Figure S4 in the online Supporting Information).

Figure 8 displays the results for the slope–area diagram for the orographic precipitation and spatially varied solar radiation scenario for both vegetated and bare soil conditions. As seen in Figure 8 and discussed above (Figure 7f), the relative steepness of slopes in the windward and leeward flanks varies with contributing area when considering the effect of coevolving vegetation. However, for the case of landscapes with bare soil, this reversal does not occur, the leeward slopes are steeper than those at the windward flank for all contributing areas, because in this case there is no protective effect of vegetation.



**FIGURE 8** Slope–area plot for orographic precipitation with bare soil and vegetated domains for the windward and leeward slopes. ‘Lee B’ and ‘wind B’ represent the mean slopes of the bare soil on the leeward and windward sides of the domain, respectively. ‘Wind V’ and ‘Lee V’ represent the mean slopes of the windward and leeward sides of the domain, respectively.

Figure 9 shows the discharge for the windward and leeward sides using the orographic precipitation with the spatially varied solar radiation setting for both the vegetated and bare soil domains. As seen in



**FIGURE 9** Mean discharge–area plot for orographic precipitation with bare soil and vegetated domain. ‘Lee B’ and ‘wind B’ represent the mean discharge on the leeward and windward sides of the bare soil domain, respectively. ‘Wind V’ and ‘Lee V’ represent the mean discharge of the windward and leeward sides of the vegetated domain, respectively.

this figure, the discharge for the windward side of the bare soil domain is higher than the windward side of the vegetated soil domain. Similarly, the discharge for the leeward side of the bare soil case is higher than that of the leeward side for the vegetated soil case. The discharge is also higher on the windward side for both the bare soil domain and the vegetated domain in comparison to their respective leeward sides.

## 5 | DISCUSSION

Our results suggest that drainage network, aspect, and elevation controls are the three main drivers of landscape vegetation patterns, but their relative dominance varies for the different scenarios considered. The effect of the drainage network is dominant for the setting that assumes uniform solar radiation and uniform precipitation. In this case, a higher vegetation cover fraction is obtained for the channels (higher drainage areas) than the hillslopes, which highlights the network control on vegetation cover induced by flow concentration and its associated increase in soil moisture availability. This result is consistent with the findings of previous studies (Collins & Bras, 2010; Ivanov et al., 2008; Yetemen, Istanbuluoglu, Flores-Cervantes, et al., 2015).

When the effect of aspect is considered, its impact becomes dominant and masks the effect of flow accumulation induced by the drainage network on the resulting vegetation cover patterns, for all of the precipitation settings analysed (i.e. uniform, elevation control, and orographic precipitation). Differences in incoming solar radiation on NFS and SFS dominate the spatial distribution of vegetation cover. This result is consistent with field observations reporting that incoming solar radiation leads to sparser vegetation cover on SFS than NFS (Bass et al., 2017; Broza et al., 2004; Del-Toro-Guerrero et al., 2016) and in agreement with previous modelling studies considering the effect of aspect under uniform precipitation (Caylor et al., 2004;

Flores-Cervantes et al., 2014; Gutiérrez-Jurado et al., 2013; Hinckley et al., 2014; Srivastava et al., 2019; Yetemen, Istanbuluoglu, Flores-Cervantes, et al., 2015; Zou et al., 2007).

However, the additional effects of both elevation and orographic precipitation controls have not been considered in previous modelling studies, even though elevation and orography substantially affect precipitation patterns (Dettinger et al., 2004; Giroto et al., 2014; Hanson, 2001; Kirchner et al., 2014; Knowles et al., 2015). For instance, Dettinger et al. (2004) reported differences in precipitation amounts with elevation, with amounts 30 times higher at the top than at the base of a mountain range. The inclusion of elevation control led to a clear increase in vegetation with elevation (which had implications for the coevolving landforms as will be explained later). In real-world catchments, Kumari et al. (2020) reported a strong control of aspect and elevation on vegetation distribution. We have included an example of those real-world catchments in the online Supporting Information (Figure S5), where we analysed greenness as a function of elevation in Gabilan Mesa, California. The vegetation greenness versus elevation patterns obtained from this analysis (Figure S6) were similar to the results from our model (Figure 4b). The effect of orographic precipitation led to significant differences in vegetation cover between windward (displaying higher cover) and leeward slopes (lower cover), particularly for the case in which the effects of aspect and slope on radiation were considered, in agreement with field observations (Chen et al., 1997; Giambelluca et al., 2011). For this case, NFS and SFS on the windward and leeward slopes displayed highly distinct patterns of vegetation cover, which also reflected the effect of elevation and aspect.

Previous observational evidence highlighted the importance of understanding and considering the combined effects of slope aspect (insolation) and predominant wind direction on vegetation patterns on the windward and leeward mountain flanks (Fernández-Palacios & de Nicolás, 1995; Rozas et al., 2011). Substantial differences in vegetation growth between windward and leeward slopes of the mountain flanks on Tenerife, Canary Islands have been observed (Rozas et al., 2011). This is in agreement with previous findings that Canary pine forests on windward and leeward slopes are separate ecosystems, each with their own dynamics and environmental constraints (Fernández-Palacios & de Nicolás, 1995). For instance, the pine forests occupy the highest part of the island between elevations of 1300–2000 m on the windward slopes and 700–2200 m on the leeward slopes.

Our results indeed reflect the importance of accounting for these combined effects, with the emergence of a lower vegetation cover fraction for NFS on the leeward side than for NFS on the windward side of the mountain. However, denser vegetation cover emerges on SFS of the windward side of the mountain flank. Indeed, additional studies based on field observations also suggest that the effect of orography (windward vs leeward locations) on vegetation patterns can sometimes be more important than that of aspect, as shown in the studies by Dettinger et al. (2004) and Lundquist et al. (2010) at Sierra Nevada, California.

In terms of the implications of orographic precipitation on landform evolution, our results from the bare soil simulations show that the windward side of the domain is gentler than the leeward side as the latter receives less rainfall, leading to lower erosion and steeper

slopes for landform evolution equilibrium conditions (i.e. erosion equals tectonic uplift). These results are consistent with those from previous modelling studies (Anders et al., 2008; Goren et al., 2014; Han et al., 2015; Paik & Kim, 2021; Zavala et al., 2020). The results for divide migration for bare soil conditions are also in agreement with results from previous studies (Anders et al., 2008; Bonnet, 2009), in which the windward side of the domain is found to be gentler for low contributing areas (such as those in the divide), and the drainage divide is displaced from the centre of the domain towards the leeward side (Anders et al., 2008; Bonnet, 2009; Giachetta et al., 2014).

Unlike previous modelling work, the current study also analysed differences in divide migration for a vegetated domain. Interestingly, the pattern of migration of the vegetated domain remained consistent with that of the bare soil domain, and therefore consistent with results from previous studies (i.e. with a displacement from the centre of the domain towards the leeward flank). We found that the reason for this shift is that the vegetation cover close to the divide is similar on both sides, but the runoff discharge on the windward side is higher than on the leeward side due to rainshadow effects (Figure 9). This leads to higher shear stress due to increased runoff on the windward side, that overrides the effect of vegetation protection (similar on both sides) on erosion and leads to milder slopes on this flank (Istanbulluoglu & Bras, 2005; Istanbulluoglu et al., 2008; Yetemen, Istanbulluoglu, Flores-Cervantes, et al., 2015). This interpretation is consistent with a previous study in the Central Andes, showing that the enhanced runoff is expected to increase erosion potential and result in lower hillslope gradients in equilibrium landscapes (Jeffery et al., 2014). Although plot-scale experiments and modelling studies demonstrate continued increases in erosion with decreasing vegetation cover (e.g. Nearing et al., 2015), in real-world scenarios, sparse vegetation often correlates with low precipitation, limited bioturbation, and potentially lower soil-production rates, which altogether minimizes sediment transport (Acosta et al., 2015).

At dynamic equilibrium, steeper slopes emerge on the leeward side of the vegetated landscape close to the divide. This topographic asymmetry between the leeward and windward sides is found to be more pronounced for aspect-controlled and orographic-precipitation conditions. Though the effect of increased runoff on the windward side dominates at higher elevations, we found a reversal of dominant mechanisms for lower areas. In these locations, the difference in vegetation cover between windward and leeward flanks of the mountain becomes more pronounced and the effect of vegetation protection dominates differences in erosion (over the effect of runoff) and the resulting slopes that are slightly steeper on the windward than those on the leeward flanks. A limitation of the current modelling study is given by the assumption that potential evapotranspiration does not vary as a function of elevation. The effect of cooler temperatures and lower PET at higher elevations can have an additional indirect effect on water stress and therefore affect vegetation distribution. However, scaling the PET with elevation would reinforce the patterns identified in this study on vegetation distribution and divide migration. Further, it is worth mentioning that, in the current model setup, grass is considered as the only vegetation type, which may result in the underestimation of mean vegetation cover. Different vegetation types with different phenology are likely to occur in slopes with different aspects.

## 6 | CONCLUSIONS

In this study, the CHILD LEM coupled with the vegetation dynamic component BGM is used to improve our current understanding of the roles of elevation control and orographic precipitation on the coevolution of landforms and aspect-controlled vegetation in semi-arid ecosystems. Model simulations were run for 800 000 years on an initially two-sided landscape subjected to the effect of different solar radiation and precipitation settings. The results from the simulations showed that for uniform precipitation and uniform solar radiation, the vegetation pattern is controlled by the effect of the drainage network, as higher soil moisture occurs on channels driving higher vegetation cover. However, when the effect of aspect on radiation is considered, this effect overrides drainage control and becomes dominant, resulting in an aspect-controlled vegetation distribution with higher cover on SFS. If elevation control on precipitation is included, its effect dominates that of the drainage network for the case with constant radiation and the vegetation pattern is characterized by a higher vegetation cover at higher elevations. However, if elevation control on precipitation is combined with spatially varying solar radiation, both effects determine the emerging vegetation patterns.

Rainshadow effects, included in the orographic precipitation simulations, result in a denser vegetation cover on the windward than on the leeward side of the domain when uniform solar radiation is considered. When considering the effects of both orographic precipitation and spatially varied solar radiation, a more complex relationship emerged between vegetation and elevation. At higher elevations, where precipitation is similar on both sides, the aspect control of solar radiation effect dominates, leading to denser vegetation cover on NFS on the leeward side compared with SFS on the windward side of the domain.

Differences in the coevolution of landforms and vegetation under different precipitation and solar radiation settings are also significant and lead to various degrees of erosion on opposing slopes, resulting in topographic asymmetry and divide migration. There is negligible divide migration for the case of uniform precipitation and uniform solar radiation; however, a slight shift of the divide is seen when accounting for the effect of spatially varied solar radiation. This is due to the fact that aspect drives vegetation differences that lead to topographic asymmetry across the domain. Including elevation control precipitation reinforces aspect differences in vegetation, resulting in a more noticeable shifting of the divide. The highest divide migration is observed when the orographic precipitation effects are incorporated because the slopes of the windward side of the mountain flank are gentler than the leeward slopes of the mountain flank. Surprisingly, the divide migration in the vegetated landscapes is similar to that obtained for bare soil landscapes. This occurs because the vegetation cover close to the divide is similar on both sides, but the runoff discharge on the windward side is higher than on the leeward side due to rainshadow effects. However, for the lower areas away from the divide the simulations with vegetation differ from the bare soil results, indicating the importance of differences in vegetation on windward and leeward flanks.

The key contribution of this landform evolution study is the advancement in knowledge of the distribution of the vegetation cover fraction on the windward and leeward sides of a mountain under the influence of orographic precipitation, and its effects on the generation

of topographic asymmetry in semi-arid ecosystems. This link between climatic, vegetation, and geomorphic processes emphasizes the coupled nature of the earth system and represents an under-explored area at the interface between climate, erosion, and vegetation.

## ACKNOWLEDGEMENTS

This research was funded by the University of Newcastle Postgraduate Research Scholarship (UNRSC) 50:50 (A. Srivastava). Additional funding was provided by the Australian Research Council through grants FT140100610 and DP140104178 (P.M. Saco) and the Scientific and Technological Research Council of Turkey (TUBITAK) through grant 118C329 (O. Yetemen).

## CONFLICT OF INTEREST

The authors declare no conflict of interest.

## AUTHOR CONTRIBUTIONS

**Ankur Srivastava:** Conceptualization, Methodology, Investigation, Writing - original draft, Writing - review & editing. **Omer Yetemen:** Conceptualization, Methodology, Investigation, Writing - review & editing. **Patricia M. Saco:** Conceptualization, Methodology, Investigation, Writing - original draft, Writing - review & editing. **Jose F. Rodriguez:** Conceptualization, Methodology, Investigation, Writing - review & editing. **Nikul Kumari:** Conceptualization, Methodology, Investigation, Writing - original draft, Writing - review & editing. **Kwok P. Chun:** Conceptualization, Writing - review & editing.

## DATA AVAILABILITY STATEMENT

The CHILD model simulation results are available from the corresponding author upon reasonable request.

## ORCID

Ankur Srivastava  <https://orcid.org/0000-0002-3963-265X>

Omer Yetemen  <https://orcid.org/0000-0003-1593-3519>

Patricia M. Saco  <https://orcid.org/0000-0002-2478-3025>

Jose F. Rodriguez  <https://orcid.org/0000-0002-1472-1277>

Nikul Kumari  <https://orcid.org/0000-0003-3765-529X>

Kwok P. Chun  <https://orcid.org/0000-0001-9873-6240>

## REFERENCES

- Acosta, V.T., Schildgen, T.F., Clarke, B.A., Scherler, D., Bookhagen, B., Wittmann, H., von Blanckenburg, F. & Strecker, M.R. (2015) Effect of vegetation cover on millennial-scale landscape denudation rates in East Africa. *Lithosphere*, 7(4), 408–420. Available from: <https://doi.org/10.1130/L402.1>
- Anders, A.M., Ne, A., Roe, G.H. & Montgomery, D.R. (2008) Influence of precipitation phase on the form of mountain ranges. *Geology*, 36(6), 479–482. Available from: <https://doi.org/10.1130/G24821A.1>
- Anders, A.M., Roe, G., Durran, D.R. & Minder, J.R. (2006) Small-scale spatial gradients in climatological precipitation on the Olympic peninsula. *Journal of Hydrometeorology*, 8(5), 1068–1081. Available from: <https://doi.org/10.1175/JHM610.1>
- Baartman, J.E., Temme, A.J. & Saco, P.M. (2018) The effect of landform variation on vegetation patterning and related sediment dynamics. *Earth Surface Processes and Landforms*, 43(10), 2121–2135. Available from: <https://doi.org/10.1002/esp.4377>
- Bass, B., Cardenas, M.B. & Befus, K.M. (2017) Seasonal shifts in soil moisture throughout a semiarid hillslope ecotone during drought: A geoelectrical view. *Vadose Zone Journal*, 16(2), 1–17. Available from: <https://doi.org/10.2136/vzj2016.11.0108>
- Bierman, P.R., Reuter, J.M., Pavich, M., Gellis, A.C., Caffee, M.W. & Larsen, J. (2005) Using cosmogenic nuclides to contrast rates of erosion and sediment yield in a semi-arid, arroyo-dominated landscape, Rio Puerco Basin, New Mexico. *Earth Surface Processes and Landforms*, 30(8), 935–953. Available from: <https://doi.org/10.1002/esp.1255>
- Bonnet, S. (2009) Shrinking and splitting of drainage basins in orogenic landscapes from the migration of the main drainage divide. *Nature Geoscience*, 2(12), 897–897. Available from: <https://doi.org/10.1038/Ngeo700>
- Broza, M., Poliakov, D., Gruia, M. & Bretfeld, G. (2004) Soil collembolan communities on north- and south-facing slopes of an eastern Mediterranean valley. *Pedobiologia*, 48(5–6), 537–543. Available from: <https://doi.org/10.1016/j.pedobi.2004.07.007>
- Carson, M.A. & Kirkby, M.J. (1972) *Hillslope Form and Process*. Cambridge: Cambridge University Press.
- Caylor, K.K., Scanlon, T.M. & Rodriguez-Iturbe, I. (2004) Feasible optimality of vegetation patterns in river basins. *Geophysical Research Letters*, 31, L13502.
- Chaboureaud, J.-P. (2008) A midlatitude precipitating cloud database validated with satellite observations. *Journal of Applied Meteorology and Climatology*, 47(5), 1337–1353. Available from: <https://doi.org/10.1175/2007JAMC1731.1>
- Chen, Z.S., Hsieh, C.F., Jiang, F.Y., Hsieh, T.H. & Sun, I.F. (1997) Relations of soil properties to topography and vegetation in a subtropical rain forest in southern Taiwan. *Plant Ecology*, 132(2), 229–241. Available from: <https://doi.org/10.1023/A:1009762704553>
- Clapp, E.M., Bierman, P.R., Nichols, K.K., Pavich, M. & Caffee, M. (2001) Rates of sediment supply to arroyos from upland erosion determined using in situ produced cosmogenic <sup>10</sup>Be and <sup>26</sup>Al. *Quaternary Research*, 55(2), 235–245. Available from: <https://doi.org/10.1006/qres.2000.2211>
- Clift, P.D., Hodges, K.I.P.V., Heslop, D., Hannigan, R., Long, H.V.A.N. & Calves, G. (2008) Correlation of Himalayan exhumation rates and Asian monsoon intensity. *Nature Geoscience*, 17(12), 875–880. Available from: <https://doi.org/10.1038/ngeo351>
- Colberg, J.S. & Anders, A.M. (2014) Geomorphology numerical modelling of spatially-variable precipitation and passive margin escarpment evolution. *Geomorphology*, 207, 203–212. Available from: <https://doi.org/10.1016/j.geomorph.2013.11.006>
- Collins, D.B.G. & Bras, R.L. (2008) Climatic control of sediment yield in dry lands following climate and land cover change. *Water Resources Research*, 44(Jun), 1–8. Available from: <https://doi.org/10.1029/2007WR006474>
- Collins, D.B.G. & Bras, R.L. (2010) Climatic and ecological controls of equilibrium drainage density, relief, and channel concavity in dry lands. *Water Resources Research*, 46(4), 1–18. Available from: <https://doi.org/10.1029/2009WR008615>
- Collins, D.B.G., Bras, R.L. & Tucker, G.E. (2004) Modeling the effects of vegetation-erosion coupling on landscape evolution. *Journal of Geophysical Research - Earth Surface*, 109(F3), F03004. Available from: <https://doi.org/10.1029/2003JF000028>
- Del-Toro-Guerrero, F.J., Hinojosa-Corona, A. & Kretzschmar, T.G. (2016) A comparative study of NDVI values between north- and south-facing slopes in a semiarid mountainous region. *IEEE Journal of Selected Topics in Applied Earth Observations and Remote Sensing*, 9(12), 5350–5356. Available from: <https://doi.org/10.1109/JSTARS.2016.2618393>
- Dethier, D.P. (2001) Pleistocene incision rates in the western United States calibrated using Lava Creek B tephra. *Geology*, 29(9), 783–786. Available from: [https://doi.org/10.1130/0091-7613\(2001\)029<0783:PIRITW>2.0.CO;2](https://doi.org/10.1130/0091-7613(2001)029<0783:PIRITW>2.0.CO;2)
- Dettinger, M., Redmond, K. & Cayan, D. (2004) Winter orographic precipitation ratios in the Sierra Nevada: Large-scale atmospheric circulations and hydrologic consequences. *Journal of Hydrometeorology*, 5(6), 1102–1116. Available from: <https://doi.org/10.1175/JHM-390.1>

- Dietrich, W.E. & Perron, J.T. (2006) The search for a topographic signature of life. *Nature*, 439(7075), 411–418.
- Eagleson, P. (1978) Introduction to water balance dynamics. *Water Resources Research*, 14(5), 705–712. Available from: <https://doi.org/10.1029/WR014i005p00705>
- Farquhar, G.D., Ehleringer, J.R. & Hubick, K.T. (1989) Carbon isotope discrimination and photosynthesis. *Annual Review of Plant Physiology and Plant Molecular Biology*, 40, 503–537. Available from: <https://doi.org/10.1146/annurev.pp.40.060189.002443>
- Fernández-Palacios, J.M. & de Nicolás, J.P. (1995) Altitudinal pattern of vegetation variation on Tenerife. *Journal of Vegetation Science*, 6(2), 183–190. Available from: <https://doi.org/10.2307/3236213>
- Ferrier, K.L., Huppert, K.L. & Perron, J.T. (2013) Climatic control of bedrock river incision. *Nature*, 496(7444), 206–209. Available from: <https://doi.org/10.1038/nature11982>
- Flores-Cervantes, J.H., Istanbuluoglu, E., Vivoni, E.R., Holifield Collins, C. D. & Bras, R.L. (2014) A geomorphic perspective on terrain-modulated organization of vegetation productivity: Analysis in two semiarid grassland ecosystems in southwestern United States. *Ecohydrology*, 7(2), 242–257. Available from: <https://doi.org/10.1002/eco.1333>
- Garreaud, R., Falvey, M. & Montecinos, A. (2016) Orographic precipitation in coastal southern Chile: Mean distribution, temporal variability, and linear contribution. *Journal of Hydrometeorology*, 17(4), 1185–1202. Available from: <https://doi.org/10.1175/JHM-D-15-0170.1>
- Gasparini, N.M., Bras, R.L., Tucker, G.E., Rice, S.P., Roy, A.G. & Rhoads, B.L. (2008) Numerical predictions of the sensitivity of grain size and channel slope to an increase in precipitation. In: Rice, S.P., Roy, A. G. & Rhoads, B.L. (Eds.) *River Confluences, Tributaries and the Fluvial Network*. New York: Wiley, pp. 367–394.
- Giachetta, E., Refice, A., Capolongo, D., Gasparini, N.M. & Pazzaglia, F.J. (2014) Orogen-scale drainage network evolution and response to erodibility changes: Insights from numerical experiments. *Earth Surface Processes and Landforms*, 39(9), 1259–1268. Available from: <https://doi.org/10.1002/esp.3579>
- Giambelluca, T.W., DeLay, J.K., Nullet, M.A., Scholl, M.A. & Gingerich, S.B. (2011) Canopy water balance of windward and leeward Hawaiian cloud forests on Haleakalā, Maui, Hawai'i. *Hydrological Processes*, 25(3), 438–447. Available from: <https://doi.org/10.1002/hyp.7738>
- Giroto, M., Cortés, G., Margulis, S.A. & Durand, M. (2014) Examining spatial and temporal variability in snow water equivalent using a 27-year reanalysis: Kern River watershed, Sierra Nevada. *Water Resources Research*, 50(8), 6713–6734.
- Goren, L., Willett, S.D. & Braun, J. (2014) Coupled numerical-analytical approach to landscape evolution modelling. *Earth Surface Processes and Landforms*, 545(4), 522–545. Available from: <https://doi.org/10.1002/esp.3514>
- Guan, H., Wilson, J.L. & Makhnin, O. (2005) Geostatistical mapping of mountain precipitation incorporating auto searched effects. *Journal of Hydrometeorology*, 6(6), 1018–1031. Available from: <https://doi.org/10.1175/JHM448.1>
- Gutiérrez-Jurado, H.A., Vivoni, E.R., Cikoski, C., Harrison, B.J., Bras, R.L. & Istanbuluoglu, E. (2013) On the observed ecohydrologic dynamics of a semi-arid basin with aspect-delimited ecosystems. *Water Resources Research*, 49(12), 8263–8284.
- Han, J., Gasparini, N.M. & Johnson, J.P.L. (2015) Measuring the imprint of orographic rainfall gradients on the morphology of steady-state numerical fluvial landscapes. *Earth Surface Processes and Landforms*, 40(10), 1334–1350. Available from: <https://doi.org/10.1002/esp.3723>
- Han, J., Gasparini, N.M., Johnson, J.P.L. & Murphy, B.P. (2014) Modeling the influence of rainfall gradients on discharge, bedrock erodibility, and river profile evolution, with application to the Big Island, Hawai'i. *Journal of Geophysical Research – Earth Surface*, 119(6), 1418–1440.
- Hanson, C.L. (2001) Long-term climate database, Reynolds Creek Experimental Watershed, Idaho, United States. *Water Resources Research*, 37(11), 2839–2841.
- Hinckley, E.L.S., Ebel, B.A., Barnes, R.T., Anderson, R.S., Williams, M.W. & Anderson, S.P. (2014) Aspect control of water movement on hillslopes near the rain–snow transition of the Colorado Front Range. *Hydrological Processes*, 28(1), 74–85. Available from: <https://doi.org/10.1002/hyp.9549>
- Houze, R.A., Jr. (2012) Orographic effects on precipitating clouds. *Reviews of Geophysics*, 50(2012), 1–47.
- Istanbuluoglu, E. & Bras, R.L. (2005) Vegetation-modulated landscape evolution: Effects of vegetation on landscape processes, drainage density, and topography. *Journal of Geophysical Research – Earth Surface*, 110, 1–19. Available from: <https://doi.org/10.1029/2004JF000249>
- Istanbuluoglu, E., Wang, T. & Wedin, D.A. (2012) Evaluation of ecohydrologic model parsimony at local and regional scales in a semi-arid grassland ecosystem. *Ecohydrology*, 5(1), 121–142.
- Istanbuluoglu, E., Yetemen, O., Vivoni, E.R., Gutie, H.A. & Bras, R.L. (2008) Eco-geomorphic implications of hillslope aspect: Inferences from analysis of landscape morphology in Central New Mexico. *Geophysical Research Letters*, 35(2), 1–6. Available from: <https://doi.org/10.1029/2008GL034477>
- Ivanov, V.Y., Bras, R.L. & Curtis, D.C. (2007) A weather generator for hydrological, ecological, and agricultural applications. *Water Resources Research*, 43(10), W10406. Available from: <https://doi.org/10.1029/2006WR005364>
- Ivanov, V.Y., Bras, R.L. & Vivoni, E.R. (2008) Vegetation–hydrology dynamics in complex terrain of semiarid areas: 2. Energy–water controls of vegetation spatiotemporal dynamics and topographic niches of favorability. *Water Resources Research*, 44(3), W03430. Available from: <https://doi.org/10.1029/2006WR005595>
- Jeffery, M.L., Yanites, B.J., Poulsen, C.J. & Ehlers, T.A. (2014) Vegetation precipitation controls on Central Andean topography. *Journal of Geophysical Research – Earth Surface*, 119(6), 1354–1375. Available from: <https://doi.org/10.1002/2013JF002919>
- Kirchner, P.B., Bales, R.C., Molotch, N.P., Flanagan, J. & Guo, Q. (2014) LiDAR measurement of seasonal snow accumulation along an elevation gradient in the southern Sierra Nevada, California. *Hydrology and Earth System Sciences*, 18(10), 4261–4275. Available from: <https://doi.org/10.5194/hess-18-4261-2014>
- Kirkby, M. (1995) Modelling the links between vegetation and landforms. *Geomorphology*, 13(1–4), 319–335. Available from: [https://doi.org/10.1016/0169-555X\(95\)00065-D](https://doi.org/10.1016/0169-555X(95)00065-D)
- Kirkby, M.J., Atkinson, K. & Lockwood, J. (1990) *Aspect, Vegetation Cover and Erosion on Semi-arid Hillslopes*. New York: Wiley.
- Kirshbaum, D.J. & Smith, R.B. (2008) Temperature and moist-stability effects on midlatitude orographic precipitation. *Quarterly Journal of the Royal Meteorological Society*, 1199(634), 1183–1199. Available from: <https://doi.org/10.1002/qj.274>
- Knowles, J.F., Harpold, A.A., Cowie, R., Zeliff, M., Barnard, H.R., Burns, S. P., Blanken, P.D., Morse, J.F. & Williams, M.W. (2015) The relative contributions of alpine and subalpine ecosystems to the water balance of a mountainous, headwater catchment. *Hydrological Processes*, 29(22), 4794–4808. Available from: <https://doi.org/10.1002/hyp.10526>
- Kumari, N., Saco, P.M., Rodriguez, J.F., Johnstone, S.A., Srivastava, A., Chun, K.P. & Yetemen, O. (2020) The grass is not always greener on the other side: Seasonal reversal of vegetation greenness in aspect-driven semi-arid ecosystems. *Geophysical Research Letters*, 47(15), e2020GL088918. Available from: <https://doi.org/10.1029/2020GL088918>
- Kumari N, Yetemen O, Srivastava A, Rodriguez JF, Saco PM. 2019. The spatio-temporal NDVI analysis for two different Australian catchments. In Proceedings of the 23rd International Congress on Modeling and Simulation (MODSIM2019), Canberra, Australia; 958–964. <https://doi.org/10.36334/modsim.2019.K3.kumari>
- Langbein, W.B. & Schumm, S. (1958) Yield of sediment in relation to mean annual precipitation. *Transactions of the American Geophysical Union*, 39(6), 1076–1084. Available from: <https://doi.org/10.1029/TR039i006p01076>
- Lee T.J. 1992. *The impact of vegetation on the atmospheric boundary layer and convective storms*, PhD thesis, Colorado State University, Fort Collins, CO.
- Luce, C.H., Abatzoglou, J.T. & Holden, Z.A. (2013) The missing mountain water: Slower. *Science*, 342(Dec), 1360–1365.
- Lundquist, J.D., Minder, J.R., Neiman, P.J. & Sukovich, E. (2010) Relationships between barrier jet heights, orographic precipitation gradients, and streamflow in the Northern Sierra Nevada. *Journal of*

- Hydrometeorology*, 11(5), 1141–1156. Available from: <https://doi.org/10.1175/2010JHM1264.1>
- Malby, A.R., Whyatt, J.D., Timmis, R.J., Wilby, R.L. & Orr, H.G. (2007) Long-term variations in orographic rainfall: Analysis and implications for upland catchments. *Hydrological Sciences Journal*, 52(2), 276–291. Available from: <https://doi.org/10.1623/hysj.52.2.276>
- McMahon, D.R. (1998) *Soil, Landscape and Vegetation Interactions in Small Semi-arid Drainage Basin: Sevilleta National Wildlife Refuge, New Mexico*. Socorro, NM.: Nmtech.
- Minder, J.R., Mote, P.W. & Lundquist, J.D. (2010) Surface temperature lapse rates over complex terrain: Lessons from the cascade mountains. *Journal of Geophysical Research Atmospheres*, 115, 1–13.
- Moglen, G.E. & Parsons, R.M. (1998) On the sensitivity of drainage density to climate change. *Water Resources Research*, 34(4), 855–862. Available from: <https://doi.org/10.1029/97WR02709>
- Montaldo, N., Rondena, R., Albertson, J.D. & Mancini, M. (2005) Parsimonious modelling of vegetation dynamics for ecohydrologic studies of water-limited ecosystems. *Water Resources Research*, 41(10), 1–16. Available from: <https://doi.org/10.1029/2005WR004094>
- Murata, F., Hayashi, A.T. & Matsumoto, A.J. (2007) Rainfall on the Meghalaya Plateau in Northeastern India—one of the rainiest places in the world. *Natural Hazards*, 42, 391–399. Available from: <https://doi.org/10.1007/s11069-006-9084-z>
- Nearing, M.A., Unkrich, C.L., Goodrich, D.C., Nichols, M.H. & Keefer, T.O. (2015) Temporal and elevation trends in rainfall erosivity on a 149 km<sup>2</sup> watershed in a semi-arid region of the American Southwest. *International Soil and Water Conservation Research*, 3(2), 77–85.
- Osborn, H.B. (1984) Estimating precipitation in mountainous regions. *Journal of Hydraulic Engineering*, 110(12), 1859–1863. Available from: [https://doi.org/10.1061/\(ASCE\)0733-9429\(1984\)110:12\(1859\)](https://doi.org/10.1061/(ASCE)0733-9429(1984)110:12(1859))
- Paik, K. & Kim, W. (2021) Simulating the evolution of the topography–climate coupled system. *Hydrology and Earth System Sciences*, 25(5), 2459–2474. Available from: <https://doi.org/10.5194/hess-25-2459-2021>
- Pelletier, J.D., Barron-Gafford, G.A., Gutiérrez-Jurado, H., Hinckley, E.L.S., Istanbuluoglu, E., McGuire, L.A., Niu, G.Y., Poulos, M.J., Rasmussen, C., Richardson, P., Swetnam, T.L. & Tucker, G.E. (2018) Which way do you lean? Using slope aspect variations to understand Critical Zone processes and feedbacks. *Earth Surface Processes and Landforms*, 43(5), 1133–1154. Available from: <https://doi.org/10.1002/esp.4306>
- Pelletier, J.D. & Swetnam, T.L. (2017) Asymmetry of weathering-limited hillslopes: The importance of diurnal covariation in solar insolation and temperature. *Earth Surface Processes and Landforms*, 42(9), 1408–1418.
- Rata, M., Douaoui, A., Larid, M. & Douaik, A. (2020) Comparison of geostatistical interpolation methods to map annual rainfall in the Chéiff watershed, Algeria. *Theoretical and Applied Climatology*, 141(3), 1009–1024. Available from: <https://doi.org/10.1007/s00704-020-03218-z>
- Regmi, N.R., McDonald, E.V. & Rasmussen, C. (2019) Hillslope response under variable microclimate. *Earth Surface Processes and Landforms*, 44(13), 2615–2627.
- Roe, G.H. (2005) Orographic precipitation. *Annual Review of Earth and Planetary Sciences*, 33(1), 645–671. Available from: <https://doi.org/10.1146/annurev.earth.33.092203.122541>
- Roe, G.H. & Montgomery, D.R. (2002) Steady-state river profiles. *Geology*, 30(2), 143–146. Available from: [https://doi.org/10.1130/0091-7613\(2002\)030<0143:EOOPVO>2.0.CO;2](https://doi.org/10.1130/0091-7613(2002)030<0143:EOOPVO>2.0.CO;2)
- Roe, G.H., Montgomery, D.R. & Hallet, B. (2003) Orographic precipitation and the relief of mountain ranges. *Journal of Geophysical Research: Solid Earth*, 108(B6), 2315. Available from: <https://doi.org/10.1029/2001JB001521>
- Roering, J.J., Kirchner, J.W. & Dietrich, W.E. (1999) Evidence for nonlinear, diffusive sediment transport on hillslopes and implications for landscape morphology. *Water Resources Research*, 35(3), 853–870.
- Rozas, V., Pérez-de-Lis, G., García-González, I. & Arévalo, J.R. (2011) Contrasting effects of wildfire and climate on radial growth of *Pinus canariensis* on windward and leeward slopes on Tenerife, Canary Islands. *Trees – Structure and Function*, 25(5), 895–905.
- Saco, P.M. & Moreno-de las Heras, M. (2013) Ecogeomorphic coevolution of semiarid hillslopes: Emergence of banded and striped vegetation patterns through interaction of biotic and abiotic processes. *Water Resources Research*, 49(1), 115–126. Available from: <https://doi.org/10.1029/2012WR012001>
- Saco, P.M., Willgoose, G.R. & Hancock, G.R. (2007) Eco-geomorphology of banded vegetation patterns in arid and semi-arid regions. *Hydrology and Earth System Sciences Discussions*, 11(6), 1717–1730. Available from: <https://doi.org/10.5194/hess-11-1717-2007>
- Scaff, L., Rutllant, J.A., Rahn, D., Gascoin, S. & Rondanelli, R. (2017) Meteorological interpretation of orographic precipitation gradients along an Andes west slope basin at 30 S (Elqui Valley, Chile). *Journal of Hydro-meteorology*, 18(3), 713–727. Available from: <https://doi.org/10.1175/JHM-D-16-0073.1>
- Schoorl, J.M., Sonneveld, M.P.W. & Veldkamp, A. (2000) Three-dimensional landscape process modelling: The effect of DEM resolution. *Earth Surface Processes and Landforms*, 25, 1025–1034.
- Schoorl, J.M., Veldkamp, A. & Bouma, J. (2002) Modeling water and soil redistribution in a dynamic landscape context. *Soil Science Society of America Journal*, 66, 1610–1619.
- Shi, X. & Durran, D.R. (2015) Estimating the response of extreme precipitation over midlatitude mountains to global warming. *Journal of Climate*, 28(10), 4246–4262. Available from: <https://doi.org/10.1175/JCLI-D-14-00750.1>
- Small, E.E. (2005) Climatic controls on diffuse groundwater recharge in semiarid environments of the southwestern United States. *Water Resources Research*, 41(4), W04012. Available from: <https://doi.org/10.1029/2004WR003193>
- Smith, R.B. (2003) A linear upslope-time-delay model for orographic precipitation. *Journal of Hydrology*, 282(1–4), 2–9. Available from: [https://doi.org/10.1016/S0022-1694\(03\)00248-8](https://doi.org/10.1016/S0022-1694(03)00248-8)
- Smith, R.B. & Barstad, I. (2004) A linear theory of orographic precipitation. *Journal of the Atmospheric Sciences*, 61(12), 1377–1391.
- Smith, T. & Bookhagen, B. (2021) Climatic and biotic controls on topographic asymmetry at the global scale. *Journal of Geophysical Research – Earth Surface*, 126(1), e2020JF005692.
- Srivastava, A., Saco, P.M., Rodriguez, J.F., Kumari, N., Chun, K.P. & Yetemen, O. (2021) The role of landscape morphology on soil moisture variability in semi-arid ecosystems. *Hydrological Processes*, 35(1), e13990. Available from: <https://doi.org/10.1002/hyp.13990>
- Srivastava, A., Yetemen, O., Kumari, N., Saco, P.M. 2019. Aspect-controlled spatial and temporal soil moisture patterns across three different latitudes. In Proceedings of the 23rd International Congress on Modeling and Simulation (MODSIM2019), Canberra, Australia; 979–985. <https://doi.org/10.36334/modsim.2019.K6.srivastava>
- Swenson, J.J. & Waring, R.H. (2006) Modelled photosynthesis predicts woody plant richness at three geographic scales across the northwestern United States. *Global Ecology and Biogeography*, 15(5), 470–485.
- Thiede, R.C., Bookhagen, B., Arrowsmith, J.R., Sobel, E.R. & Strecker, M.R. (2004) Climatic control on rapid exhumation along the Southern Himalayan Front. *Earth and Planetary Science Letters*, 222(3–4), 791–806. Available from: <https://doi.org/10.1016/j.epsl.2004.03.015>
- Tucker, G., Lancaster, S., Gasparini, N. & Bras, R. (2001) *The Channel-Hillslope Integrated Landscape Development Model (CHILD)*. Boston, MA: Springer.
- Viviroli, D., Du, H.H., Messerli, B., Meybeck, M. & Weingartner, R. (2007) Mountains of the world, water towers for humanity: Typology, mapping, and global significance. *Water Resources Research*, 43(7), 1–13. Available from: <https://doi.org/10.1029/2006WR005653>
- Wainwright, J. (2005) Climate and climatological variations in the Jornada Experimental Range and neighbouring areas of the US Southwest. *Advances in Environmental Monitoring and Modelling*, 2, 39–110.
- Webb RH, Murov MB, Esque TC, Boyer DE, DeFalco LA, Haines DF, Oldershaw D, Scoles SJ, Thomas KA, Blainey JB, Medica PA. 2003. *Perennial vegetation data from permanent plots on the Nevada Test Site, Nye County, Nevada* (No. 2003–336). US Geological Survey: Reston, VA.



- Whipple, K.X., Kirby, E. & Brocklehurst, S.H. (1999) Geomorphic limits to climate-induced increases in topographic relief. *Nature*, 401(6748), 39–43.
- Willgoose, G., Bras, R.L. & Rodriguez-Iturbe, I. (1991a) A coupled channel network growth and hillslope evolution model: 1. Theory. *Water Resources Research*, 27, 1671–1684.
- Willgoose, G., Bras, R.L. & Rodriguez-Iturbe, I. (1991b) A coupled channel network growth and hillslope evolution model: 2. Non dimensionalization and applications. *Water Resources Research*, 27, 1685–1696.
- Willgoose, G.R. (2018) *Principles of Soilscape and Landscape Evolution*. Cambridge: Cambridge University Press.
- Yetemen, O., Istanbuluoglu, E. & Duvall, A.R. (2015) Solar radiation as a global driver of hillslope asymmetry: Insights from an ecogeomorphic landscape evolution model. *Water Resources Research*, 51(12), 9843–9861.
- Yetemen, O., Istanbuluoglu, E., Flores-Cervantes, J.H., Vivoni, E.R. & Bras, R.L. (2015) Ecohydrologic role of solar radiation on landscape evolution. *Water Resources Research*, 51(2), 1127–1157.
- Yetemen, O., Saco, P.M. & Istanbuluoglu, E. (2019) Ecohydrology controls the geomorphic response to climate change geophysical research letters. *Geophysical Research Letters*, 46(15), 8852–8861. Available from: <https://doi.org/10.1029/2019GL083874>
- Zavala, V., Carretier, S. & Bonnet, S. (2020) Influence of orographic precipitation on the topographic and erosional evolution of mountain ranges. *Basin Research*, 32(6), 1574–1599. Available from: <https://doi.org/10.1111/bre.12443>
- Zou, C.B., Barron-Gafford, G.A. & Breshears, D.D. (2007) Effects of topography and woody plant canopy cover on near-ground solar radiation: Relevant energy inputs for ecohydrology and hydrogeology. *Geophysical Research Letters*, 34(24), 1–6.

#### SUPPORTING INFORMATION

Additional supporting information can be found online in the Supporting Information section at the end of this article.

**How to cite this article:** Srivastava, A., Yetemen, O., Saco, P.M., Rodriguez, J.F., Kumari, N. & Chun, K.P. (2022) Influence of orographic precipitation on coevolving landforms and vegetation in semi-arid ecosystems. *Earth Surface Processes and Landforms*, 1–17. Available from: <https://doi.org/10.1002/esp.5427>